THE JOURNAL OF PHYSICAL CHEMISTRY B

Article

pubs.acs.org/JPCB

Combination of Transient 2D-IR Experiments and Ab Initio Computations Sheds Light on the Formation of the Charge-Transfer State in Photoexcited Carbonyl Carotenoids

Mariangela Di Donato,[†,‡,§,∥] Mireia Segado Centellas,[†,⊥] Andrea Lapini,[*,‡,§,∥] Manuela Lima,[‡,§] Francisco Avila,[#,○] Fabrizio Santoro,[*,#] Chiara Cappelli,[△] and Roberto Righini[‡,§,∥]

[‡]LENS (European Laboratory for Nonlinear Spectroscopy) via N. Carrara 1, 50019 Sesto Fiorentino (FI), Italy

[§]INO (Istituto Nazionale di Ottica), Largo Fermi 6, 50125 Firenze, Italy

[∥]Dipartimento di Chimica "Ugo Schiff", Università di Firenze, via della Lastruccia 13, 50019 Sesto Fiorentino (FI), Italy

[⊥]Scuola Normale Superiore, Piazza dei Cavalieri 7, I-56126 Pisa, Italy

[△]Dipartimento di Chimica e Chimica Industriale, Università di Pisa, via Risorgimento 35, I-56126 Pisa, Italy

[#]CNR-Consiglio Nazionale delle Ricerche, Istituto di Chimica dei Composti Organo Metallici (ICCOM-CNR), UOS di Pisa, Area della Ricerca, via G. Moruzzi 1, I-56124 Pisa, Italy

[○]University of Málaga, Physical Chemistry, Faculty of Science, Málaga, 29071, Spain

Supporting Information

ABSTRACT: The excited state dynamics of carbonyl carotenoids is very complex because of the coupling of single- and doubly excited states and the possible involvement of intramolecular charge-transfer (ICT) states. In this contribution we employ ultrafast infrared spectroscopy and theoretical computations to investigate the relaxation dynamics of *trans*-8′-apo-*β*-carotenal occurring on the picosecond time scale, after excitation in the S_2 state. In a (slightly) polar solvent like chloroform, one-dimensional (T1D-IR) and two-dimensional (T2D-IR) transient infrared spectroscopy reveal spectral components with characteristic frequencies and lifetimes that are not observed in nonpolar solvents (cyclohexane). Combining experimental evidence with an analysis of CASPT2//CASSCF ground and excited state minima and energy profiles, complemented with TDDFT calculations in gas phase and in solvent, we propose a photochemical decay mechanism for this system where only the bright single-excited $1B_u^+$ and the dark double-excited $2A_g^-$ states are involved. Specifically, the initially populated $1B_u^+$ relaxes toward $2A_g^-$ in 200 fs. In a nonpolar solvent $2A_g^-$ decays to the ground state (GS) in 25 ps. In polar solvents, distortions along twisting modes of the chain promote a repopulation of the $1B_u^+$ state which then quickly relaxes to the GS (18 ps in chloroform). The $1B_u^+$ state has a high electric dipole and is the main contributor to the charge-transfer state involved in the dynamics in polar solvents. The $2A_g^- \rightarrow 1B_u^+$ population transfer is evidenced by a cross peak on the T2D-IR map revealing that the motions along the same stretching of the conjugated chain on the $2A_g^-$ and $1B_u^+$ states are coupled.

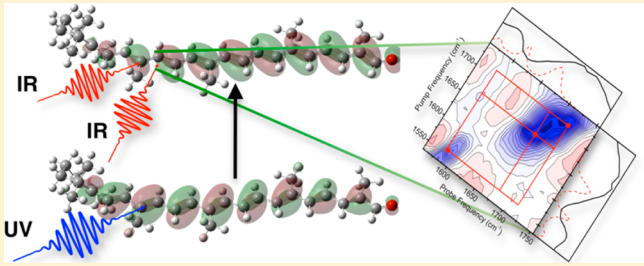

1. INTRODUCTION

Carotenoids, together with chlorophylls, are among the most abundant pigments in nature. In photosynthesis they cover important roles in light harvesting[1−3] and photoprotection,[4,5] but they are also implied in other fundamental life processes where they act either as quenchers of harmful singlet oxygen and reactive radicals or as pigment precursors or photoprotective elements in vision.[6] Recent studies have also proven the utility of carotenoids as components of photovoltaic[7] and artificial photosynthetic systems,[8,9] and it is clear that the design of efficient devices cannot prescind from a detailed understanding of the photophysics of these dyes and its dependence on structural motives, like the polyene length and the effect of possible substituents. Indeed, the photophysics of carotenoids is extremely complex, and has been the subject of many experimental investigations, including a number of time-resolved measurements, mostly focused so far on the analysis of the visible spectral range.[10−13]

Formulating a consistent picture of the relaxation pathway of electronic energy in carotenoids is actually a difficult task, mostly because of the poor knowledge of the nature and energies of the low lying excited states. The excited state dynamics in carotenoids is often discussed taking as a reference an idealized C_{2h} polyene symmetry. According to this description, the first excited state S_1, of $2A_g^-$ symmetry, cannot be populated by one photon excitation from the $1A_g^-$ ground

Received: June 3, 2014
Revised: July 22, 2014
Published: July 22, 2014

state.[14] Absorption of light in the visible spectral range (450−550 nm) thus populates the second low-lying excited state, S_2, of B_u^+ symmetry. Following the one photon excitation to S_2, the excited state dynamics is dominated by an ultrafast $S_2 \rightarrow S_1$ relaxation, occurring in 100−300 fs.[12,13] The S_1 state then relaxes to the ground state (GS) with a lifetime ranging between 50 and 200 ps,[12] whose exact value depends on several factors like conjugation length and solvent polarity. This is just a simplified scheme: the actual picture is in reality more complex, not only because the order of the $1B_u^+$ and $2A_g^-$ is not always well assessed and depends on the length of the polyene chain,[13] but also because the C_{2h} symmetry rules are not strictly applicable to carotenoids. As a result, other low-lying excited states, close in energy to S_2 and S_1, are present.[10,13,15] For instance, very recently 2D electronic spectra have allowed to document the involvement of the dark $1B_u^-$ state of carotenoids in the light-harvesting complex of purple bacteria, suggesting its role in enhancing the efficiency of the excitation energy transfer (EET).[3]

For carotenoids made structurally asymmetric by the presence of one electron withdrawing group, like the molecule considered in this study, the energy relaxation pathway is furthermore complicated, and their excited state properties depend on the polarity of the environment.[16−19] In a polar environment the short-chain apocarotenals exhibit a strong reduction of the excited-state lifetime, which is not observed in long-chain ones.[16] This phenomenon is explained with the involvement of an intramolecular charge transfer (ICT) state, whose existence has been inferred from previous experimental evidence.[17,18]

Although the role of an ICT excited state in the relaxation of carbonyl carotenoids is so far accepted in the literature, its exact electronic nature and the mechanism of its formation are not yet clear. The label "S_1/ICT", commonly adopted in literature, is rather confusing since "S_1" may indicate either the lowest adiabatic state or the parent state before coupling with ICT;[19−21] this state however might have an electronic configuration more similar to either $2A_g^-$ or $1B_u^+$. Different models have been proposed to interpret the huge amount of information, often difficult to reconcile within a unified kinetic scheme, obtained from ultrafast spectroscopic experiments on such systems and, in particular, on the naturally occurring carotenoid peridinin.[19,21−23] The major questions still remaining unsolved are (*i*) whether the long-lasting S_1 state has $2A_g^-$ or $1B_u^+$ parentage and a partial ICT character[24] (two-states model) or if the ICT state exists as a well-defined state, with an electronic configuration clearly distinguished from $2A_g^-$ and $1B_u^+$ state (three states model). In the latter case, ICT might be only slightly coupled with $2A_g^-$ or $1B_u^+$ and possibly establishing a solvent dependent equilibrium with them (*ii*, weak-coupling);[17,21,23,25] or alternatively (*iii*, strong-coupling) there could be a solvent dependent strong-mixing between the S_1 and the ICT state, giving rise to a combined state (generally indicated as S_1/ICT).[19] While the mixing mechanism (hypothesis (*iii*)) is widely accepted, a recent study on *trans*-8′-apo-*β*-carotenal in methanol[26] proposes that stimulated emission (usually attributed to ICT) and additional transient absorption bands (not attributed to ICT) occur from a single adiabatic state (S_1) characterized by an asymmetric electronic distribution, whose population is enhanced in polar solvents (hypothesis (*i*): two-state model). Therefore, the explanation of the shortening of the lifetime in polar solvents, the existence and nature of the ICT state and the mechanism by which this state is populated is still controversial.

Unveiling the decay pathway and the nature of such ICT state in carbonyl carotenoids is important for a detailed understanding of the mechanism of excitation energy transfer (EET) in several natural systems, as algae's light-harvesting complexes (containing peridinin)[13] and for the design of efficient carotenoids-based systems for photovoltaic applications and artificial photosynthesis. It has been shown, in fact, that the pathway through the ICT state enhances the EET from peridinin to chlorophyll.[27,28] In this sense, understanding the photoexcited behavior of carotenoids is a prerequisite to control it and to design and synthesize species with optimal performance in photosynthetic devices. On an even more general ground, the study of the photophysics of carotenoids also has a relevant methodological interest since subtle interplay of several electronic states, structural rearrangements and solvent effects, challenge the available experimental and theoretical methodologies, providing an ideal playground for testing the potentiality of novel experimental and theoretical approaches.

The considerations outlined above prompted us to undertake a joint experimental and theoretical study on the excited-state dynamics of a specific apocarotenal, *trans*-8′-apo-*β*-carotenal (in short 8-apocarotenal), in nonpolar and polar solution. The chemical structure and atom labeling of 8-apocarotenal are shown in Figure 1.

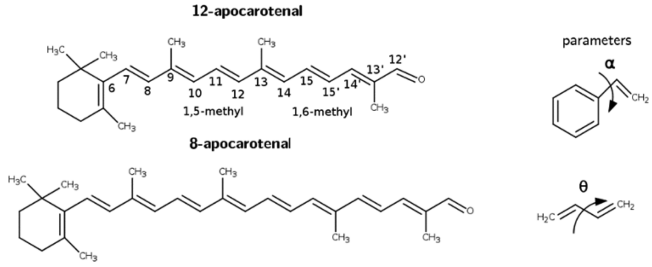

Figure 1. Structures of 12-apocarotenal and 8-apocarotenal and geometrical parameters defined.

As we will show in the following, this system is particularly interesting since, because of the length of the conjugated chain, the $2A_g^-$ and $1B_u^+$ states exhibit similar energies in a large region of the nuclear configurations, so that they establish a delicate equilibrium that can be altered by the solvent.

In our work we employ ultrafast nonlinear spectroscopic methods based on pulse sequences in the vis and mid-IR spectral regions, along with multiconfigurational and density functional theory computations, in order to shed further light on the details of the complex de-excitation process.

Although previous studies based on visible-pump/mid-IR-probe technique (T1D-IR) spectroscopy have been reported,[29−31] two-dimensional IR spectroscopy, preceded by vis ultrafast excitation (T2D-IR), was never applied to the study of carotenoids. The application of IR two-dimensional spectroscopy allows to investigate the coupling between different vibrational modes and to resolve structural changes on the picoseconds time scale.[32] In its more common application, 2D-IR is used to study the evolution of molecular systems in the electronic ground state, but its extension to the study of nonequilibrium states allows obtaining important structural information also on the electronic excited states

dx.doi.org/10.1021/jp505473j | J. Phys. Chem. B 2014, 118, 9613−9630

populated by the visible pump.[33] By opportunely scanning the time delay between the visible and infrared pump pulses, such technique allows to retrieve information on the coupled dynamics of multiple excited states along the relaxation path.

Concerning quantum chemical computations, density functional theory (DFT) gives reliable results for electronic and vibrational ground-state properties; time-dependent density functional theory (TDDFT) is a cost-effective methodology that provides reliable excitation spectra both in the gas phase and in a solvent.[34] For the system under investigation, however, double excitations play a relevant role, so that TD-DFT level appears to be inadequate. Nevertheless, the combination of DFT and (MS-)CASPT2//CASSCF computations permits us to investigate the nature of the excited states and the photochemical reaction mechanism, achieving a detailed picture of vibrational and electronic properties of apocarotenals that goes beyond the limits of both methods. More in detail, in this work we calculated the excited states of 8-apocarotenal in the gas phase and investigated how they are affected by the solvent, thus, obtaining a robust theoretical basis for interpreting its spectroscopic properties and understanding its photochemical behavior. Since the size of 8-apocarotenal molecule challenges MS-CASPT2//CASSCF computations and make prohibitive an extensive exploration of the potential energy surfaces (PESs), such an exploration was performed for the more affordable *trans*-12′-apo-*β*-carotenal (12-apocarotenal, Figure 1).

Our joint experimental and theoretical investigation provides new insights into the decay mechanism of carotenoids, allowing us to individuate vibrational marks of different electronic states in polar solvents that are not observed in nonpolar ones. Furthermore, based on our experimental and theoretical results, we are able to suggest a sound physical mechanism for the formation of the ICT state in polar solvents. Our study supports the two-state model (hypothesis (*i*)); we propose that, in polar solvents, after the initial decay to the $2A_g^-$ state, structural deformations induce a repopulation of the $1B_u^+$ state, the latter being the dominant contributor to the so-called ICT state, which eventually relaxes to the ground state.

2. MATERIALS AND METHODS

2.1. Experimental Methods. *trans*-*β*-Apo-8′-carotenal was purchased from SIGMA and used without further purification. For all infrared measurements, the sample was prepared by dissolving the *trans*-*β*-apo-8′-carotenal in cyclohexane or chloroform and squeezing about 40 μL of solution between two calcium fluoride windows (2 mm thickness) separated by a 50 μm (100 μm for the cychlohexane solution) Teflon spacer. The optical density (OD) at the excitation wavelength was about 0.4 for all samples.

For time-resolved measurements, the output of Ti:sapphire oscillator/regenerative amplifier, operating at 1 kHz, (Legend Elite, Coherent) was split to pump a home-built optical parametric amplifier (OPA) with difference frequency generation and a commercial optical parametric amplifier (TOPAS, Light Conversion). The spectral width of both OPAs was about ∼200 cm^{-1} in the mid-IR. The visible excitation pulse was generated by frequency doubling another portion of the Legend output in a BBO crystal to generate the pump-pulses at 400 nm (∼6 nm fwhm) which were attenuated to provide 100−300 nJ and focused to a spot of ∼150 μm in diameter. In case of T1D-IR measurements, a moveable delay line made it possible to control the time-of-arrival difference of the pump and probe pulses up to 1.8 ns. The pump beam polarization was set to the magic angle with respect to the probe beam by means of a $\lambda/2$ plate; the measurements were taken in two partially overlapping spectral windows, covering the spectral region 1450−1800 cm^{-1}.

2D-IR spectra were collected in the dynamic hole-burning configuration, involving two infrared pulses. A narrow band pump pulse, whose frequency is scanned through one of the frequency axes (the pump axis), and a broad band probe pulse that, once passed through a monochromator, determines the second frequency axis (probe axis), generate the two-dimensional spectral map.[32,35,36] Narrow band infrared pump pulses were obtained by sending the output of the TOPAS OPA through a Fabry−Perot element, which allows obtaining pulses with spectral width of about 15 cm^{-1}. In the nonequilibrium extension of the 2D-IR measurement, an additional visible pump pulse, centered at 400 nm, prepares the system in the S_2 electronically excited state. By scanning the t_{vis} time delay between the visible and infrared pump pulses (see Scheme 1 for the pulse sequence employed), it is possible to collect 2D-IR snapshots of the system while the electronic excited state relaxes.

Scheme 1. Pulse Sequence Used to Record the T2D-IR Spectra

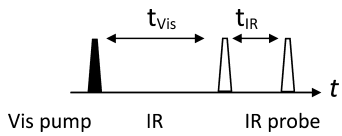

Ground state equilibrium 2D spectra, as well as excited state nonequilibrium T2D-IR spectra, were recorded, respectively, with parallel polarization between the infrared pump and probe pulses and with parallel polarization between the Vis-IR-IR pulses. The sample was moved with a home-built scanner to refresh the solution and avoid photodegradation. A fraction of the probe pulse was split off before the sample and used as a reference. After the sample, both probe and reference were spectrally dispersed in a spectrometer (TRIAX 180, HORIBA JobinYvon) and imaged separately on a 32 channels double array HgCdTe (MCT) detector (InfraRed Associated Inc., Florida, U.S.A.) with a sampling resolution of 6 cm^{-1}. The integrity of the sample was checked by FTIR (Bruker Alpha-T) and visible absorption (PerkinElmer LAMBDA 950) before and after the time-resolved measurements.

2.2. Experimental Data Analysis. T1D-IR spectra have been analyzed by applying a combined approach, consisting of singular values decomposition (SVD)[37−39] and the simultaneous fitting of all the collected kinetic traces (global analysis, GA). The aim of global analysis is to decompose the two-way data matrix into time-independent spectra and wavelength independent kinetics.[40] Once the number of components is identified through the SVD decomposition, the second step involves the parametrization of the time evolution of the spectral components. This was accomplished by assuming first-order kinetics, describing the overall temporal evolution as the sum or combination of exponential functions. Global analysis was performed using the GLOTARAN package (http://glotaran.org)[41,42] and employing a linear unidirectional "sequential" model.

2.3. Quantum Chemical Computations. Equilibrium geometries on both ground and excited electronic states were

dx.doi.org/10.1021/jp505473j | J. Phys. Chem. B 2014, 118, 9613−9630

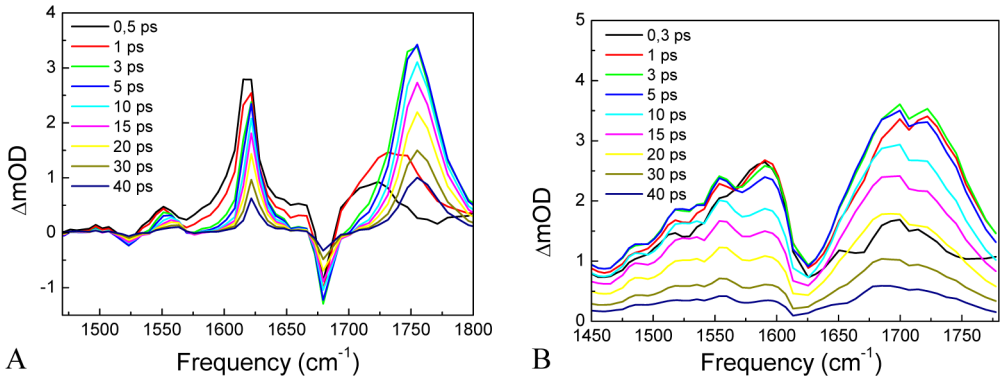

Figure 2. T1D-IR spectra, collected at different vis-pump/mid-IR-probe delays measured in (a) cyclohexane and (b) chloroform in the 1450−1800 cm^{-1} spectral region.

computed both by the DFT (TD-DFT) method employing the long-range corrected CAM-B3LYP functional[43] and by using the complete active space self-consistent field (CASSCF)[44] in conjunction with the 6-31G(d) basis set (458 basis functions). Geometry optimizations were performed in nonredundant internal coordinates for CASSCF and in redundant internal coordinates for DFT and TD-DFT, by computation of analytical energy gradients. Ground state harmonic vibrational frequencies were obtained both at CASSCF and DFT levels from analytic energy second derivatives; TD-DFT excited-state Hessians were computed from the numerical differentiation of the analytical energy gradients. Single point excited state energies were computed with the TD-DFT,[45] with the second-order multiconfigurational perturbation theory (CASPT2),[46] and with the multistate extension of CASPT2 (MS-CASPT2).[47] Together with the target system 8-apocarotenal, we studied also 12-apocarotenal as a more affordable model system on which it has been possible to perform extensive PES explorations and, through preliminary tests, to establish a suitable computational protocol. In such a way, by balancing accuracy and computational cost, we obtained a reliable description of the states involved in the decay process (see Supporting Information (SI)). For 12-apocarotenal energies in the $1A_g^-$, $2A_g^-$, and $1B_u^+$ minima were refined with the larger ANO-s basis set (4s3p1d/2s1p contraction scheme, 638 basis functions). It is noteworthy that CASPT2//CASSCF methodology has allowed a detailed understanding of the photophysics of the protonated Schiff base of retinal (15-apocarotenal),[28,48] the chromophore of rhodopsin that is involved in the mechanism of molecular vision.[49,50]

To set up the active space, two occupied and two virtual π MOs in 12-apocarotenal and four occupied and four virtual π MOs 8-apocarotenal were excluded from the complete π-space, yielding a 12 electrons distributed in 12 orbitals (See figure SI1 in Supporting Information for further details). TD-DFT calculations (see SI) ruled out any significant involvement of $n\pi^*$ excitations, which are known to play a dominant role in the decay of the shorter-chain carotenoids in nonpolar solvents.[51]

In principle, possibly large interactions of the CASSCF wave functions at the MS-CASPT2 level make the results sensitive to the number of states included in the state averaged (SA) CASSCF reference wave functions. Test calculations (see Tables SI5, SI8, SI9, and SI10 in the Supporting Information) at ground-state and excited-state geometry minima show that the necessary stability of the energies of the states, as well as of their compositions in terms of configuration state functions (CSF) is ensured by averaging the lowest eight states (SA8).

All valence electrons were correlated in CASPT2 calculations by using the complete Fock matrix in the definition of the zero order Hamiltonian, together with an imaginary level shift of 0.2 au in order to avoid the incorporation of intruder states.[52] Carbon and oxygen 1s core electrons were kept frozen. Interaction of CASSCF states via dynamic correlation was taken into account with MS-CASPT2. The resulting perturbed modified (PM) CAS (PM-CAS-CI) wave functions were also obtained. The analysis of natural orbital occupancies of these functions provided the necessary information to characterize the nature of the different electronic states.

Transition dipole moments were computed with the CAS state interaction (CAS-SI)[53] method employing the perturbatively modified CASSCF functions (PM-CAS-CI) obtained as a linear combination of the states in the MS-CASPT2 calculation.

We obtained the frequency shift of relevant normal modes in the excited states by scanning the CASSCF PES along the ground-state normal modes (see section 7 of Supporting Information, SI) and fitting it with quadratic functions. Tests performed on this procedure showed that, in the GS, it delivers harmonic frequencies very close to those computed analytically. Linearly interpolated internal reaction coordinate (LIIRC) paths were calculated at the CASPT2/CASSCF/6-31G(d) level between critical geometries of interest in several PES to individuate a plausible decay mechanism.

Solvent effects were accounted for by a polarizable continuum model (PCM).[54,55] Due to the delicate mixing of states, it was not possible to converge PCM//CASSCF calculations. However, major solvent effects are expected for the single-excitation $1B_u^+$ state, characterized by a large electric dipole, and since it is properly described by TD-DFT, they were investigated with this method, adopting the state-specific implementation of PCM (SS-PCM).[56−59]

Calculations were performed with the Gaussian09[60] (DFT and TD-DFT) and Molcas 7.4[61] (CASSCF) programs. For CASPT2 calculations, we use the default IPEA zero-order Hamiltonian.[62]

3. RESULTS

3.1. Experimental Results. Probing the system with broadband mid-IR pulses after visible excitation represents a powerful tool for detecting and monitoring the dynamics of apocarotenals. Key modes to be monitored are C═C and C═O stretching vibrations since they are expected to undergo

dx.doi.org/10.1021/jp505473j | J. Phys. Chem. B 2014, 118, 9613−9630

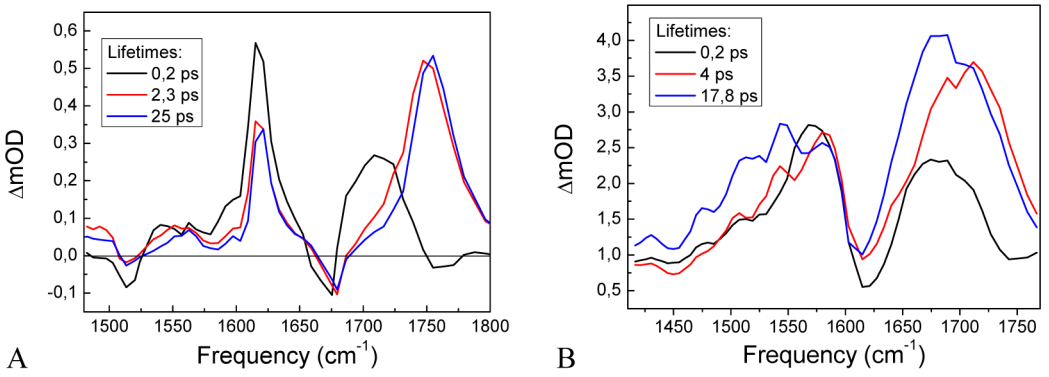

Figure 3. EADS (evolution associated decay spectra) obtained by globally analyzing the kinetic traces collected in (A) cyclohexane and (B) chloroform upon excitation at 400 nm. In both cases three kinetic components are extracted from the fit whose lifetimes are, respectively, 200 fs, 2.3 ps, and 25 ps in cyclohexane and 200 fs, 4 ps, and 17.8 ps in chloroform.

relevant frequency shifts upon excitation and internal conversion, and can therefore be used to identify the populated electronic state. Light absorption induces variations in bond order and consequent modifications of the nuclear structure, which are also reflected in shifts of the frequencies of the normal modes undergoing the major displacements.

3.1.1. Transient One-Dimensional Infrared (T1D-IR). We measured transient one-dimensional infrared spectra (T1D-IR) of 8-carotenal in two different solvents, cyclohexane which is completely nonpolar, and chloroform, which is instead slightly polar. The transient spectra were collected by exciting the sample with a 400 nm pulse and probing in the mid-IR, between 1450 and 1800 cm^{-1}.

In the spectra registered in cyclohexane (Figure 2A) it is possible to recognize negative bleaching bands, due to ground state depletion, and positive bands due to excited state absorption. The spectra in chloroform are instead characterized by much broader positive signals (see Figure 2B), which completely cover the bleaching contributions, as previously reported.[29−31] This striking diversity suggests that the excited states populated in the two analyzed solvents may have different electronic structures, or at least that the solvent strongly influences the charge distribution of the electronic excited states of this carotenoid.

3.1.2. Evolution Associated Difference Spectra (EADS). In order to extract the kinetic constants describing the dynamic evolution of the system, we analyzed the transient data by applying a combined approach, consisting of singular values decomposition (SVD)[37−39] and of simultaneous fitting of all the collected kinetic traces (global analysis). In both solvents three kinetic components are required to satisfactory fit the data: one extremely rapid, whose lifetime has been fixed at 200 fs (being at the limit of our time resolution), an intermediate 2−4 ps component and, finally, a longer, solvent-dependent, picosecond decay component.

Besides the time constants, global analysis allows extracting the spectral profiles associated with the dynamic processes occurring in the systems, the so-called EADS; those obtained from the spectra in cyclohexane and chloroform are reported in Figure 3A and B, respectively.

In both solvents the first EADS (black lines in Figure 3A,B), whose lifetime was fixed at 200 fs, reflects the fast decay of the initially populated excited state S_2 ($1B_u^+$) to S_1. The highest frequency absorption band (peaked at 1680 cm^{-1} in chloroform and 1710 cm^{-1} in cyclohexane) is also the broadest in both solvents; in the lower frequency region, the bands observed in cyclohexane are rather sharp, while in chloroform they are very broad and largely overlapped. The high frequency excited state absorption band gains intensity as the delay time increases and upshifts in both solvents giving rise in the second EADS to an intense band peaked at about 1750 cm^{-1} in cyclohexane and to a broad absorption at 1715 cm^{-1} in chloroform (Figure 3A,B, red line). In the low frequency part of the spectrum (1650−1450 cm^{-1} in cyclohexane, 1600−1450 cm^{-1} in chloroform) changes with time delay are less evident: the excited state absorption in cyclohexane shows intensity decay; only a small band shape change is observed in chloroform. Finally, after 2.3 ps in cyclohexane (4 ps in chloroform), the second EADS evolves into the last spectral component. We notice that in the third EADS the excited state absorption band located in the high frequency region (blue line in Figure 3A,B) shifts to opposite direction in the two solvents: in cyclohexane there is a slight blue-shift (ca. 5 cm^{-1}), which can be attributed to vibrational cooling, while in chloroform the band gains intensity on the red side (peak at 1685 cm^{-1}). This could imply that in polar solvents two components, with different rise times, underlay this broad absorption, as suggested by the inspection of the kinetic traces reported in Figure 4. The lifetime of the last spectral component reflects the dependence on the solvent polarity of the $S_1 \rightarrow$ GS recovery time, which is shorter in chloroform as compared to cyclohexane. The extracted

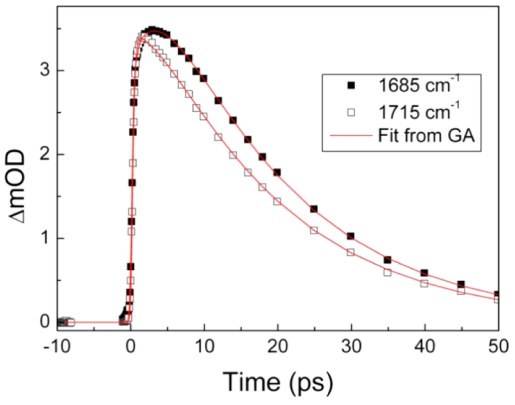

Figure 4. Normalized kinetic traces measured for 8-apocarotenal in chloroform solution, respectively, at 1685 (closed symbols) and 1715 cm^{-1} (open symbols), together with the fit obtained by global analysis (red lines).

dx.doi.org/10.1021/jp505473j | J. Phys. Chem. B 2014, 118, 9613−9630

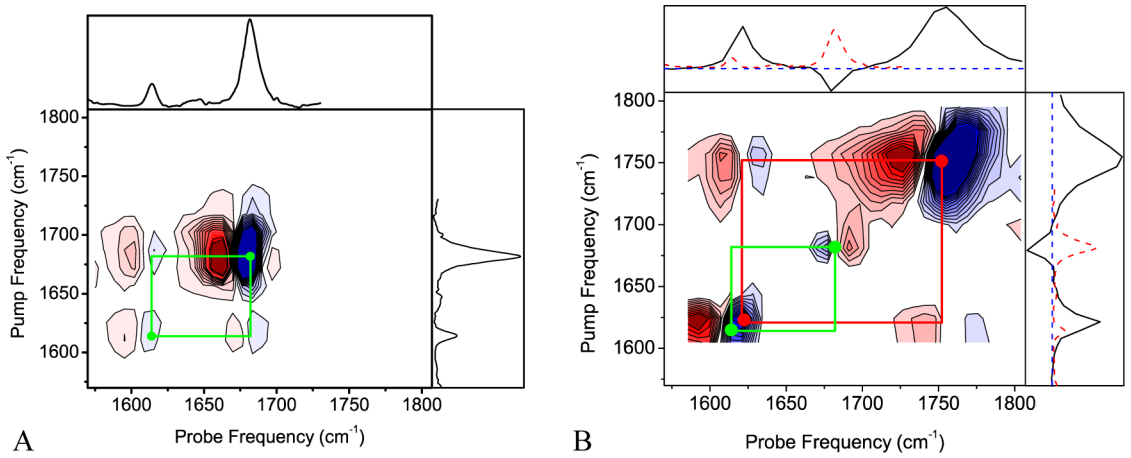

Figure 5. (A) Ground state 2D-IR spectrum of 8-apocarotenal in cyclohexane, registered with an IR-pump-IR-probe delay of 500 fs. (B) Corresponding excited state spectrum registered 3 ps after the excitation with a 400 nm pulse. Negative lobes are shown in blue and positive in red.

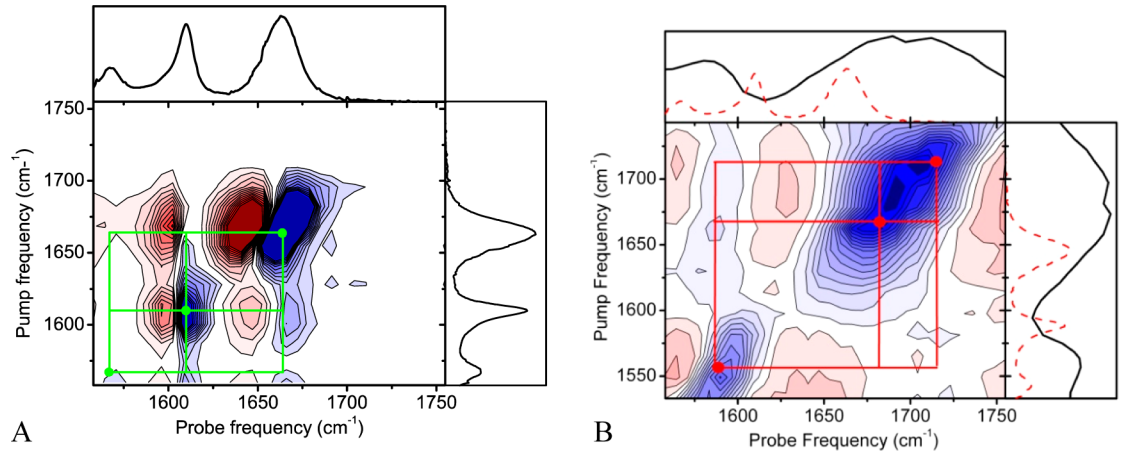

Figure 6. (A) 2D-IR spectrum of 8-apocarotenal in chloroform, registered with an IR-pump-IR-probe delay of 500 fs. (B) Corresponding excited state spectrum registered 3 ps after the excitation with a 400 nm pulse.

lifetimes of S_1, about 18 ps in chloroform and 25 ps in cyclohexane, agree well with previously reported values.[16]

3.1.3. Transient Two-Dimensional Vibrational Spectra (T2D-IR). Additional information on the excited state dynamics can be obtained from the measure of nonequilibrium 2D-IR spectra. Figure 5 reports the ground state 2D-IR spectrum of 8-carotenal in cyclohexane and the corresponding T2D-IR spectrum, recorded with 3 ps delay from the visible excitation pulse.

In the ground state spectrum, absorption and bleaching peaks along the diagonal correspond to the vibrational modes observed in the FTIR spectrum, reported on top of Figure 5A. Bleaching and excited state absorptions bands (the latter are red-shifted because of anharmonicity) are visible for both the C═O (1680 cm^{-1}) and one of the C═C (1614 cm^{-1}) stretching modes. Assignment of these modes is robust as it is discussed in section 3.3. Cross peaks due to the anharmonic coupling between the two modes are also evident, and are connected to the corresponding diagonal peaks by green lines. It is well-known that an elongated and tilted shape of 2D-IR bands is indicative for inhomogeneous broadening.[32,63] In this case, bands are vertically elongated, indicating that the inhomogeneous broadening is negligibly small. In Figure 5B we show the corresponding 2D-IR spectrum of the excited state. For reference, on top of the 2D-IR map we report the transient T1D-IR spectrum (black full line) measured 3 ps after the arrival of the 400 nm pump and the ground state FTIR spectrum (red dotted line). In this case, vibrational signals attributable both to the electronic ground and excited states appear along the diagonal. Signals corresponding to vibrations of the electronic excited state consist of negative bleaching lobes (blue) and of downshifted excited state absorption positive lobes (red). The signs are inverted for the vibrational bands of the electronic ground state.

The T2D-IR spectrum in cyclohexane (Figure 5B) is relatively simple to interpret: the resonances are well separated and correspond to the bands observed in the linear spectrum of the excited state (same figure, black line). Consistent with the transient T1D-IR spectrum, the 2D map shows diagonal peaks in the regions around 1750 and 1600 cm^{-1}. As discussed in section 3.3, these two bands can be assigned, respectively, to the upshifted C═C symmetric stretching and the downshifted C═O stretching in the $2A_g^-$ state. The cross peaks between these excited state resonances are well resolved; in the figure the red lines point out the connections to the respective diagonal peaks.

When repeated on the chloroform solution, the experiment yields a significantly different result, as shown in Figure 6.

Remarkable differences are already observed in the ground state spectrum (Figure 6A), where the bands appear

dx.doi.org/10.1021/jp505473j | J. Phys. Chem. B 2014, 118, 9613−9630

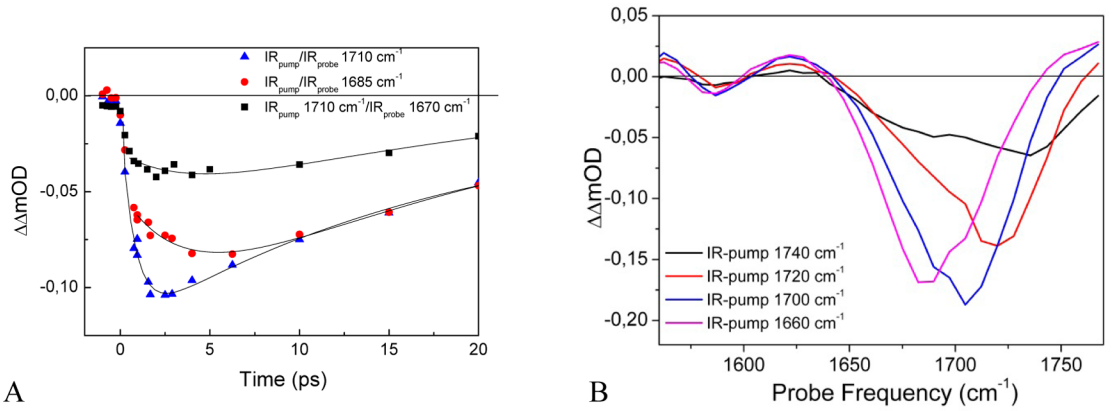

Figure 7. (A) Kinetic traces of the diagonal peaks recorded at 1685 cm^{-1} (red circles) and 1715 cm^{-1} (triangles) and of the cross peak (black squares) recorded with IR_{pump} at 1710 cm^{-1}/IR_{probe} at 1670 cm^{-1}. The t_{vis} was varied between −10 and 20 ps, with the IR_{pump}/IR_{probe} delay fixed at 500 fs. The black lines are biexponential fits to the experimental data (excluding the initial 500 fs delay time). The fitting parameters are τ_1 = 3.7 ps and τ_2 = 18.5 ps for the diagonal peak at 1685 cm^{-1}; τ_1 = 0.78 ps and τ_2 = 18.5 ps for the diagonal peak at 1710 cm^{-1}; τ_1 = 3.8 ps and τ_2 = 19.5 ps for the cross peak. (B) Cuts along different IR-pump frequencies with t_{vis} = 3 ps and t_{IR} = 500 fs.

significantly broader than those measured in cyclohexane. The diagonal peak corresponding to the C═O stretching mode (bleaching at 1660 cm^{-1}, Figure 6A) shows an appreciable degree of inhomogeneity,[32] probably reflecting the conformational disorder of the carbonyl moiety, which can assume multiple orientations depending on the interactions with the polar solvent molecules.

The 2D-IR spectrum of the excited state in chloroform (Figure 6B) is remarkably different from that measured in cyclohexane; it is actually very informative of the time evolution of the excitation in the first few picoseconds. First, three distinct peaks show up on the diagonal, to be contrasted to the two peaks observed in cyclohexane (Figure 5B). The lowest frequency band at 1590 cm^{-1} is attributed to the C═O stretching, while the two peaks at 1685 and 1715 cm^{-1} are both assigned to C═C symmetric stretching; for a discussion of the assignment, see section 3.3. It is highly suggestive that the last two 2D diagonal resonances measured in chloroform perfectly coincide with the maxima of the broad and structured band observed in the second and third EADS of the 1D transient spectrum (see Figure 3B). However, the sharper separation of the two peaks in the nonlinear spectrum allows us to measure the time evolution of their intensities unambiguously, selectively exciting each of the observed resonances by recording the 2D-IR maps at different delay times from the visible pump. A collection of those 2D spectra is given in SI (Figure SI16). In Figure 7 we report the kinetic traces (blue and red symbols) of the intensities of the two high frequency diagonal bands of Figure 6B as a function of the vis-pump/IR-probe delay. The two kinetic traces decay with the same time constant τ_2 = 18.5 ps, but they show a different time evolution at short delay times, with the rise time of the low frequency peak at 1685 cm^{-1} being markedly slower. In fact, a biexponential fit of the two sets of data gives an almost instantaneous rise time (within the pulse duration) for the high frequency component, while the peak at 1685 cm^{-1} grows with the time constant τ_1 = 3.7 ps. The copresence of two distinct states is further confirmed by the observation that relatively strong, well-defined off-diagonal peaks are visible in the high frequency region of the 2D spectrum in Figure 6B. A kinetic analysis of these spectral features (black symbols in Figure 7A) shows that they have the same time evolution as the 1685 cm^{-1} diagonal band, with the same rise time of 3.8 ps. The appearance of cross-peaks can be interpreted as the signature of population exchange between two distinct electronic states; it further strengthens the assignment of the 1685 and 1715 cm^{-1} diagonal bands to two different excited states populated after the direct optical excitation to $1Bu^+$ state.

These findings represent a remarkable advancement with respect to what already observed in the transient linear spectra of Figure 4, made possible by the fact that in the 2D experiment the two excited-state vibrations can be excited selectively and independently. The results summarized in Figure 6 provide clear evidence that two distinct electronic states are involved in the short-time photodynamics of 8-apocarotenal dissolved in a polar solvent like chloroform. The comparison with the results obtained for the cyclohexane solution shows that this is not the case when the carotenoid is in a nonpolar medium.

3.2. Computational Results. Besides giving an accurate description of the electronic nature of the excited state involved in the photodynamics, with the following theoretical analysis we aim at investigating the radiationless relaxation mechanisms that take place in apocarotenal. Several reasons, like for instance the analogies with the well-known case of retinal radiationless decay,[64,65] as well as the ability of other apocarotenal systems to photoisomerize,[66] prompted us to consider the possible role of torsional distortions in the deactivation path. As shown in the following, our calculations suggest that rotation around the conjugated carbonyl chain may have a crucial role in the relaxation of apocarotenal molecules.

3.2.1. Nature of Excited States in the Franck−Condon Region. Ground-state equilibrium geometries were computed at both CASSCF and CAM-B3LYP level of theory. Rotation around the torsional angle (α) between the cyclohexene ring and the polyene chain leads to the existence of different conformers. We will focus on the global minimum s-cis (notice "cis" with respect to the cyclohexene ring, the conjugated chain exhibits an all-trans arrangement), that is the most populated,[30] where α is 52.5° (CAM-B3LYP) and 68.6° (CASSCF) for 12-apocarotenal, and 52.1° (CAM-B3LYP) and 63.9° (CASSCF) for 8-apocarotenal.

The computed vertical energies and the electronic character of the excited states at the CASSCF Franck−Condon (FC) geometry, obtained at SA8-CASSCF(12,12)/6-31G(d) level,

dx.doi.org/10.1021/jp505473j | J. Phys. Chem. B 2014, 118, 9613−9630

Table 1. CASSCF(12,12), SS-CASPT2(12,12) and MS-CASPT2(12,12) Vertical Energies (E_{CAS}, E_{SS}, E_{MS}, in eV), Electric Dipole Moments (μ in Debye), and CASSCF(12,12) and MS-CASPT2(12,12) Oscillator Strengths (f_{CAS}, f_{MS}) of 12-Apocarotenal and 8-Apocarotenal. 6-31G(d) Basis Set[a]

			12-Apocarotenal			
SA8-CAS	E_{CAS} (μ)	f_{CAS}	E_{SS}	PM-CAS-CI	E_{MS}	f_{MS}
$1A_g^-$	0.00 (4.63)		0.00	$1A_g^-$	0.00	
$2A_g^-$	4.46 (5.79)	0.01	4.23	$(0.78)1B_u^+ + (0.16)2A_g^-$	3.70	1.55
$1B_u^-$	5.33 (5.04)	0.00	5.15	$(0.84)2A_g^- + (0.16)1B_u^+$	4.34	0.22
S3	5.95 (5.19)	0.12	5.71	$1B_u^-$	5.15	0.00
$1B_u^+$	5.97 (9.43)	2.56	3.96		5.87	0.01
			8-Apocarotenal			
$1A_g^-$	0.00 (5.79)		0.00	$1A_g^-$	0.00	
$2A_g^-$	3.62 (7.00)	0.06	3.23	$(0.61)1B_u^+ + (0.36)2A_g^-$	3.10	1.85
$1B_u^-$	4.38 (6.49)	0.06	4.00	$(0.60)2A_g^- + (0.33)1B_u^+$	3.29	0.88
$1B_u^+$	4.62 (11.53)	3.88	3.21	$1B_u^-$	4.05	0.04
S4	5.07 (5.56)	0.00	4.66	S4	4.68	0.00

[a]PM-CAS-CI states are described using as a reference the CASSCF ones (CI weights are reported in parentheses).

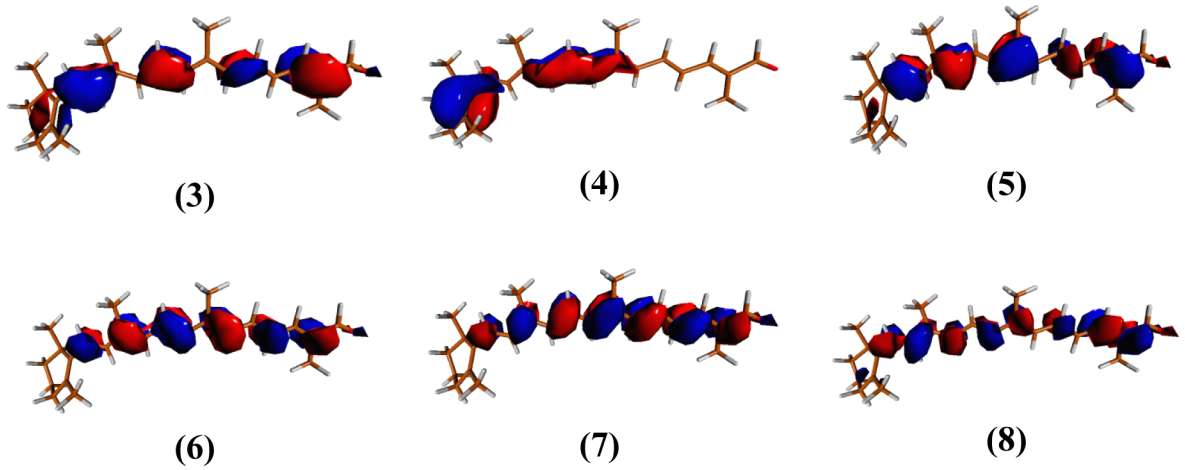

Figure 8. Active CASSCF MOs in the main transitions of low lying excited states for 12-apocarotenal. The active space comprises 12 orbitals. The MOs are labeled according to their order in the active space.

Table 2. SS-CASPT2(12,12) and MS-CASPT2(12,12) Energies (in eV) and Electric Dipole Moments (in parentheses in Debye) Computed with the ANO-s and 6-31G(d) (in italics) Basis Sets for 12-Apocarotenal at the $1A_g^-$, $2A_g^-$, and $1B_u^+$ Equilibrium Geometries Optimized at the CASSCF(12,12)/6-31G(d) Level and at the $1A_g^-$ Equilibrium Geometry Optimized at CAM-B3LYP/6-31G(d) Level

	equilibrium geometries							
states	$1A_g^-$ (CAM/B3LYP)[a]		$1A_g^-$ (CASSCF)[b]		$2A_g^-$ (CASSCF)[b]		$1B_u^+$ (CASSCF)[b]	
	SS	MS	SS	MS	SS	MS	SS	MS
$1A_g^-$	0.0[a] (5.6)	0.0[a]	0.0 (5.1)	0.0	0.39 (6.1)	0.35	−0.03 (6.6)	−0.06
$2A_g^-$	3.91 (6.5)	4.01	4.11 (6.3)	4.22	2.43 (5.7)	2.42	2.63 (6.5)	2.63
	3.95 (6.2)	*4.08*	*4.23 (5.8)*	*4.34*	*2.71 (4.8)*	*2.72*	*2.85 (5.2)*	*2.85*
$1B_u^+$	3.57 (11.5)	3.41	3.75 (10.0)	3.55	3.01 (21.9)	3.06	2.86 (20.2)	2.87
	3.73 (10.9)	*3.59*	*3.96 (9.4)*	*3.70*	*3.59 (14.4)*	*3.18*	*3.18 (15.4)*	*3.18*
$1B_u^-$	4.99 (6.4)	5.00	5.19 (5.8)	5.21	4.01 (5.8)	4.00	4.06 (6.6)	4.04
	4.87 (5.4)	*4.88*	*5.15 (5.0)*	*4.88*	*4.07 (5.1)*	*4.07*	*3.94 (5.5)*	*3.94*

[a]Energies relative to the $1A_g^-$ SS-CASPT2 and MS-CASPT2 energy at the $1A_g^-$ (CAM-B3LYP) geometry. [b]Energies relative to the $1A_g^-$ SS-CASPT2 and MS-CASPT2 energy at the $1A_g^-$ (CASSCF) geometry. The $1A_g^-$ energies at the CAM-B3LYP geometry are lower than at the CASSCF geometry by 0.17 eV (SS-CASPT2).

are listed in Table 1. The excited states are qualitatively very similar for both 12-apocarotenal and 8-apocarotenal; hereafter, CSFs are specified as $(n,m \rightarrow l,j)$, indicating an excitation from n and m to l and j CASSCF orbitals, which are sketched at the FC geometry in Figure 8. The $2A_g^-$ excited state is characterized essentially by a (6,6 → 7,7) double excitation, mixed with two single excitations, (5 → 7) and (6 → 8), that further stabilize it. The $1B_u^-$ excited state corresponds to a single-excitation (4 → 7) coupled to two double excited configurations (5,6 → 7,7) and (6,6 → 7,8). The $1B_u^+$ is

dx.doi.org/10.1021/jp505473j | J. Phys. Chem. B 2014, 118, 9613−9630

described almost completely by a single monoexcited (6 → 7) configuration (more details in Table SI2). These results are in good agreement with previous ADC(2)-x (Algebraic Diagrammatic Construction) results for polyenes.[67] It is worth pointing out that both $2A_g^-$ and $1B_u^+$ are characterized by excitations among the same occupied (6) and unoccupied (7) orbitals; this gives rise to similarities, which will be further analyzed in the next subsection.

The $1B_u^+$ state is the bright state and is characterized by a high electric dipole moment and a large oscillator strength. Notice that no other state up to the eighth CASSCF root exhibits a comparable dipole moment. When dynamical correlation is taken into account (SS-CASPT2), $1B_u^+$ becomes the first excited state both in 8-carotenal and 12-apocarotenal. Such a strong stabilization of the ionic state due to dynamical correlation has been already documented in several systems like *trans* -stilbene[68] and all-*trans*-octatetraene.[69] By comparing the calculated energies on these two systems, it is seen that both $1B_u^+$ and $2A_g^-$ states are stabilized with increasing the chain length, however the latter is more stabilized than the former, so that at the SS-CASPT2 level the $E(2A_g^-) - E(1B_u^+)$ gap is 0.27 eV for 12-apocarotenal and only 0.02 eV for 8-carotenal. This trend is in agreement with what observed in small linear polyenes.[70] For 8-carotenal, the quasi-degeneracy of the $2A_g^-$ and $1B_u^+$ states at SS-CASPT2 level explains the substantial mixing predicted by the MS-CASPT2 calculation, according to which the first two excited states S_1 and S_2 are a combination of both states, with the weights given in the second part of Table 1 (fifth column). For 12-apocarotenal, the mixing is smaller, and CASSCF and PM-CAS-CI wave functions are more similar; the mixing coefficients are shown in the first part of Table 1 (more details in Tables SI3 and SI4). Due to the limited size of the active space, the mixing of $1B_u^+$ and $2A_g^-$ states cannot be analyzed in deeper detail at this geometry but, as expected, it disappears in the excited-states minima; therefore, it will not be discussed in the following.

Table 2 compares the vertical transition energies of 12-apocarotenal computed with the 6-31G(d) and the larger ANO-s basis sets at the CASSCF $1A_g^-$ (FC) geometry. The $1B_u^+$ and $2A_g^-$ are stabilized by ∼0.2 (∼0.15) eV and ∼0.11 (∼0.11) eV, respectively, at SS-CASPT2 (MS-CASPT2) level of theory with the ANO-s basis set. Moreover, MS-CASPT2 calculations with this basis set predict a smaller mixing of the $1B_u^+$ and $2A_g^-$ states (CASSCF weights in MS-CASPT2: S1 (0.84 ($1B_u^+$) and 0.13 ($2A_g^-$)), S2 (0.81 ($2A_g^-$) and 0.13 (Bu^+)). The SS-CASPT2 energy of the $1A_g^-$ ground state is higher at the CASSCF equilibrium geometry than at the CAM-B3LYP one (by 0.17 eV for ANO-s), so that this latter represents a better approximation of the CASPT2 equilibrium geometry. Previous studies have shown that vertical energies can be sensibly dependent on the quality of the ground-state geometry.[48,71] Data in Table 2 confirms this fact showing that at the CAM-B3LYP geometry, the SS-CASPT2 (MS-CASPT2) excitation energies of $1B_u^+$ and $2A_g^-$ are lower than at the CASSCF geometry, by 0.17 (0.18) eV and 0.05 (0.07) eV, respectively. In summary, our most-accurate estimate of the $1B_u^+$ and $2A_g^-$ vertical energies in gas-phase is 3.57 and 3.91 eV (SS-CASPT2/ANO-s results at the CAM-B3LYP geometry). The $1B_u^-$ state is predicted to lie at ∼5.0 eV.

The calculations described above refer to molecules in vacuo; of course, the interaction with the solvent is expected to cause non-negligible modifications of the ground and excited states. For the investigated systems, convergence problems made it impossible to investigate solvent effects at CASSCF and CASPT2 levels of theory. Therefore, we resorted to TD-DFT calculations within the SS-PCM scheme[54,55] to compute energies and dipole moments of the $1B_u^+$ state at the FC geometry within the nonequilibrium (neq) and equilibrium (eq) solvation regimes in different solvents (and for comparison in the gas phase). We notice here that states with relevant double-excited character (like $2A_g^-$) cannot be described at the TD-DFT level. Results are reported in Table 3

Table 3. SS-PCM TDDFT/6-31G(d) Vertical Absorption Energies (E, in eV), Electric Dipole Moments (μ in Debye), and Oscillator Strengths (f) of 12-Apocarotenal and 8-Apocarotenal in Cyclohexane, Chloroform, and Methanol[a]

	12-Apocarotenal			
	E_{neq} (μ)	f_{neq}	E_{eq} (μ)	f_{eq}
	Cyclohexane			
$1A_g^-$			0.00 (6.62)	
$1B_u^+$	3.05 (16.99)	2.50	3.05 (16.92)	2.50
	Chloroform			
$1A_g^-$			0.00 (7.14)	
$1B_u^+$	3.01 (17.83)	2.49	2.87 (20.73)	2.39
	Methanol			
$1A_g^-$			0.00 (7.56)	
$1B_u^+$	3.02 (17.58)	2.51	2.69 (23.90)	2.28
	8-Apocarotenal			
	E_{neq} (μ)	f_{neq}	E_{eq} (μ)	f_{eq}
	Cyclohexane			
$1A_g^-$			0.00 (6.97)	
$1B_u^+$	2.81 (18.12)	3.376	2.81 (18.03)	3.378
	Chloroform			
$1A_g^-$			0.00 (7.43)	
$1B_u^+$	2.79 (18.93)	3.365	2.67 (22.95)	3.223
	Methanol			
$1A_g^-$			0.00 (7.78)	
$1B_u^+$	2.80 (18.35)	3.395	2.47 (27.69)	3.039

[a]Both neq and eq values are reported. The gas phase vertical energy is 3.12 eV for 12-apocarotenal and 2.91 eV for 8-apocarotenal.

for 12-apocarotenal and 8-apocarotenal. The $1B_u^+$ CASSCF state corresponds to the TD-DFT first-excited state; in fact, both states are dominated by a single HOMO−LUMO excitation, and the shapes of each of these two MOs are similar according to CASSCF and DFT calculations. The $1B_u^+$ state is also called "ionic state" in polyenes since, in a valence bond approach, it can be seen as a combination of different valence bond structures with charge separation, giving a globally neutral state;[72] in apocarotenals, the presence of the carbonyl group produces a marked asymmetry in the charge distribution. In agreement with CASSCF, TDDFT predicts this state to be characterized by a large electric dipole moment and oscillator strength. Difference density plots between $1B_u^+$ and GS states show an increase in the electronic density in the O1−C1−C2−C3 moiety in the $1B_u^+$ state (see Figure SI2 in the SI). The results reported in Table 3 also indicate that the solvent reorganization energies, obtained as differences between neq and eq data, are very similar for 8-apocarotenal and 12-apocarotenal; they are negligible in cyclohexane, but remarkable in chloroform, and even more relevant in methanol.

3.2.2. Equilibrium Geometries and Minimum Energy Paths. The minima of $2A_g^-$ and $1B_u^+$ excited states were

dx.doi.org/10.1021/jp505473j | J. Phys. Chem. B 2014, 118, 9613−9630

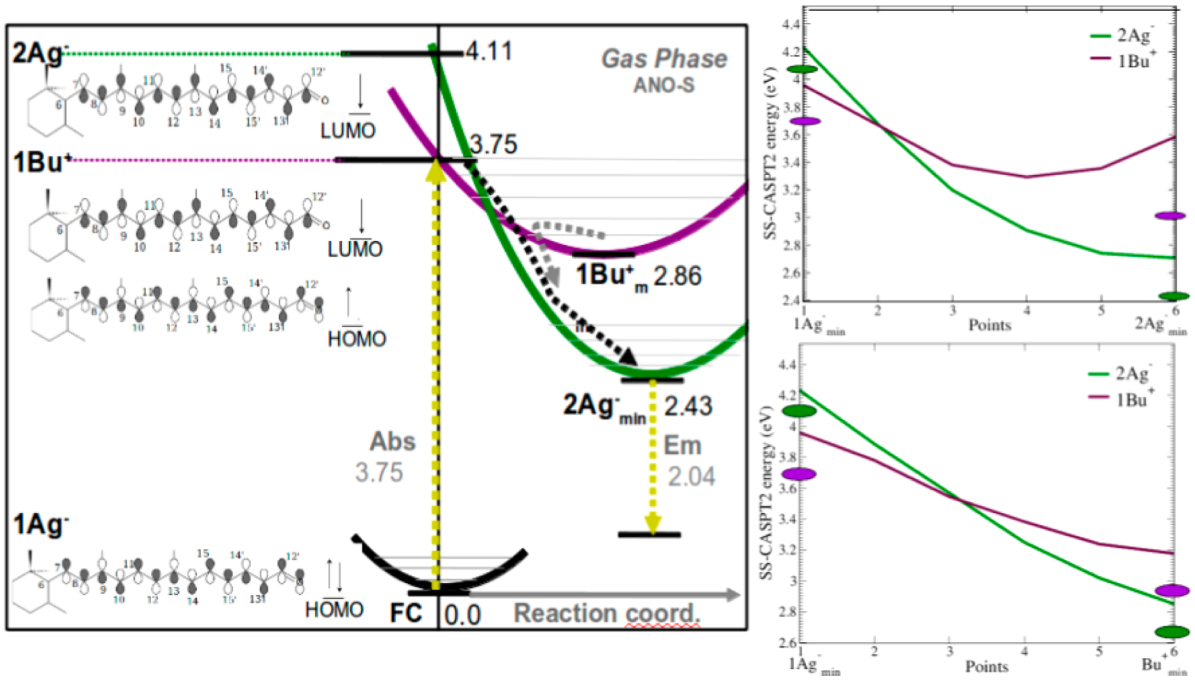

Figure 9. (Left) Schematic profile of the low-lying PESs of 12-apocarotenal and most characteristic excitations for each excited state: $2A_g^-$ in green, $1B_u^+$ in violet, absorption (Abs) and emission (Em) are depicted in yellow arrows, and proposed excited state reaction mechanism in black and gray arrows. SS-CASPT2/ANO-s energies of critical points optimized at CASSCF level (in eV) are written in black and vertical absorption and emission in gray. Notice from Table 2 that, at the CAM-B3LYP ground-state geometry, vertical excitations decrease to 3.91 ($2A_g^-$) and 3.57 eV ($1B_u^+$). (Right) LIIRC energy profiles of the $1B_u^+$ and $2A_g^-$ PES computed at SS-CASPT2//SA8-CASSCF/level of theory between the FC and the $2A_g^-$ (bottom) and $1B_u^+$(top) minima, with the smaller basis set 6-31G(d). Colored spots indicate the ANO-s energies at the stationary points.

optimized for 12-apocarotenal in gas-phase at the CASSCF (12,12)/6-31G(d) level without geometrical constraints, and the energies were refined with the larger ANO-s basis set (see Table 2 for the computed values, and Figure 9 for a schematic representation of the energy levels; geometrical parameters are reported in Figure SI3). GS, $1B_u^+$, and $2A_g^-$ minima exhibit an approximate planar arrangement of the polyene chain. With respect to the GS minimum, the equilibrium structure of the double-excited state $2A_g^-$ is displaced along a bond length alternation (BLA) mode, exhibiting a switch of the single/double bond characters, in line with what is expected from the orbitals involved in the double-excitation HOMO (6) → LUMO (7) (Figures 9 and SI1). This also explains why the same structural rearrangement (though at a lower extent) is observed also for the $1B_u^+$ minimum, where it is accompanied by an elongation of the C−O bond. A detailed analysis of the wave functions at these geometries is given in Tables SI2, SI7, SI8, SI9, and SI10. It is evident that, as in the FC point, the $1B_u^+$ state is the only one with a remarkable electric dipole moment; furthermore, the mixing predicted in the FC region at MS-CASPT2 level is much more limited in these minima, ensuring that they are nicely described at CASSCF(12,12) level and the fact that MS-CASPT2 and SS-CASPT2 energies are quite similar. Data in Table 2 show that, similarly to the behavior at the FC geometry, even at their equilibrium geometries, the excited states are stabilized by employing the larger ANO-s basis set. In the gas-phase, our most accurate estimate for the adiabatic energies (E_{AD}) of $1B_u^+$ and $2A_g^-$ states (i.e., their minimum energy with respect to the $1A_g^-$ energy in its minimum) is 2.86 and 2.43 eV, respectively (see left panel of Figure 9).

In principle, photoexcitation to the $1B_u^+$ state can trigger a variety of processes, including the relaxation to the $1B_u^+$ minimum or the de-excitation to the $2A_g^-$ state. We calculated SS-CASPT2 LIIRC paths in gas phase from the FC point to the $2A_g^-$ and $1B_u^+$ minima (right panels of Figure 9) and a path connecting these two minima (reported in Table SI11 and Figure SI4) with the more affordable 6-31G(d) basis set. The $2A_g^-$ PES exhibits a larger gradient along both of the LIIRC paths and a crossing with the $1B_u^+$ PES so that $2A_g^-$ corresponds to the S_1 adiabatic state in both minima. It is noteworthy that this prediction is not altered, adopting the larger ANO-s basis set (SS-CASPT2/ANO-s energies at the FC, $1B_u^+$, and $2A_g^-$ minima are reported as colored spots in the paths in the right panel of Figure 9; for MS-CASPT2 data, see Table 2). Such a situation is not expected to change in 8-apocarotenal, where at the FC point (see Table 1), $2A_g^-$ exhibits an additional stabilization over $1B_u^+$, making the energy gap between the two states only 0.02 eV (compared to 0.27 eV in 12-apocarotenal). Then, the decay of the initial $1B_u^+$ population toward the $2A_g^-$ minimum, suggested by the crossing of the $1B_u^+$ and $2A_g^-$ energy profiles calculated for 12-apocarotenal, should be even more favorable in 8-apocarotenal.

3.2.3. Expected Accuracy of the Computed Absolute and Relative Energies. The position of the vertical transition to the $2A_g^-$ state in apocarotenals (and carotenes) at FC point is strongly debated, since very few experimental data are available. No direct data exist for 12-carotenals, while two-photon absorption (TPA) maxima in nonpolar solvents have been reported for 8-apocarotenal and for a shorter analogue 15-apocarotenal (also known as retinal, characterized by 4 π electrons less than 12-apocarotenal). They suggest that $1B_u^+$ and $2A_g^-$ maxima are rather close in energy, being 3.36 and 3.30 eV for retinal[73] and 2.64 and 2.5 eV for 8-apocarotenal.[74,75] Our SS-CASPT2 calculations predict the opposite order, but the error on the relative stability of these

dx.doi.org/10.1021/jp505473j | J. Phys. Chem. B 2014, 118, 9613−9630

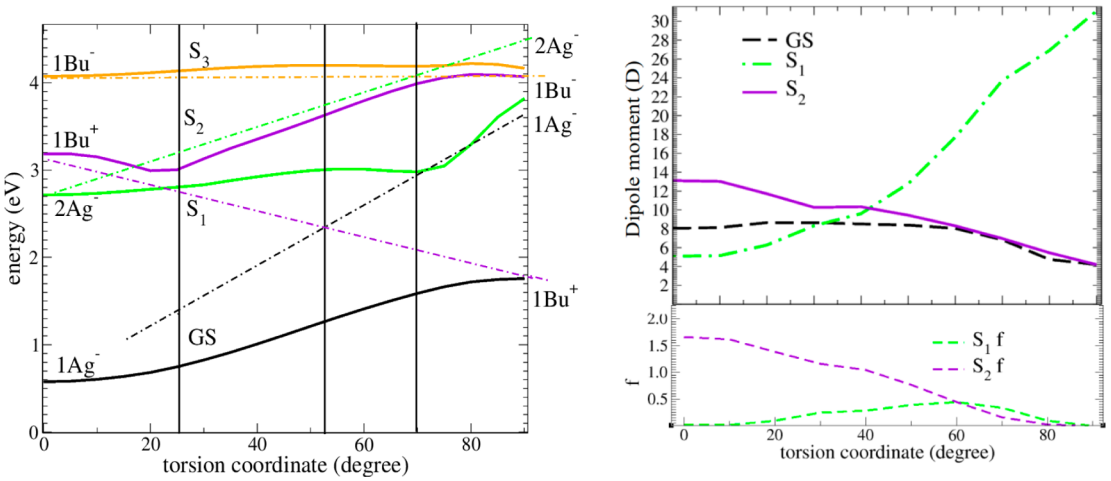

Figure 10. (Left) Torsion reaction path from the $2A_g^-$ minimum at the CASSCF/MS-CASPT2 level for 12-apocarotenal. Continuous lines represent computed adiabatic states (labeled in the figure). Dashed lines represent approximated diabatic states individuated by an the analysis of the CSF of adiabatic states (black: $1A_g^-$, green: $2A_g^-$, violet: $1Bu^+$, orange: $1B_u^-$). (Right) Electric dipole and oscillator strength (f) along the path.

two states is limited, within 0.25 eV both for 8-apocarotenal (Table 1) and for retinal (SI). On the contrary, MS-CASPT2 overemphasizes the energy splitting of $1B_u^+$ and $2A_g^-$ at FC (see Table 2), especially for retinal (see Table SI5), probably because it predicts a too strong coupling via dynamical correlation of zero order CASSCF states (Table SI6), a drawback already noticed in other systems like *trans*-stilbene.[68]

Therefore, in the following we mostly rely, at the FC point, on SS-CASPT2 energies to compare with experiment. In the excited-state minima SS and MS results almost coincide due to the small coupling. To check in detail the accuracy of our calculations, we focus on 12-apocarotenal, comparing the data computed both at the ground state and excited state minima (Table 2) with the available experimental data. A detailed analysis is given in section 4 of the SI. In summary, our best estimate for the vertical excitations of $1B_u^+$ and $2A_g^-$ at the FC point are 3.57 and 3.91 eV, respectively (SS-CASPT2/ANO-s results at CAM-B3LYP ground-state geometry). The $1B_u^+$ vertical excitation energy is therefore overestimated by ∼0.4−0.5 eV with respect to experiment (see SI). As commented above, no direct experimental data exist for the position of the vertical transition to the $2A_g^-$ state of 12-apocarotenal at FC point, and therefore, it is very difficult to estimate the error of our computations. Assuming that the vertical excitation of $2A_g^-$ state should be an intermediate between the TPA values measured for the shorter (3.30 eV for 15-apocarotenal)[73] and the longer (2.50 eV for 8-apocarotenal) analogues, roughly suggest that our FC $2A_g^-$ energies may be overestimated by about 1 eV. For 8-apocarotenal, a direct TPA measurement is possible,[74,75] and the error is actually smaller, 0.7 eV (6-31G(d) data). These remarkable inaccuracies confirm the challenge connected to get an accurate description of the energies of the dark states in linear polyenes,[76,77] evidenced even on smaller analogues as octatetraene.[69]

Despite these noticeable inaccuracies, it is important to notice that in the following we only base our discussion on the relative energies between $2A_g^-$ and $1B_u^+$. On this respect, even in the worst scenario, the relative error at the FC point is ∼0.5 eV for 12-apocarotenal, while it is considerably smaller for 8-apocarotenal (0.15 eV).[74,75] It should be also added that it is widely accepted that the initially photoexcited population decays on an ultrafast time scale on $2A_g^-$ and, notwithstanding the absolute errors discussed above, the $1B_u^+$ and $2A_g^-$ profiles in Figure 9 are in qualitative agreement with this finding, showing that the $2A_g^-$ minimum is lower in energy than the $1B_u^+$ one.

The mechanism we propose in this paper essentially concerns with the subsequent evolution of $2A_g^-$ population so that its plausibility is more directly connected with the accuracy of our calculations at the minima of the $2A_g^-$ and $1B_u^+$ states, where, luckily, a direct comparison with experiment is possible for 12-apocarotenal. The 0−0 transition of the $1A_g^- \rightarrow 2A_g^-$ spectrum has been observed at E_{00} = 2.2 eV in apolar solvents.[16] Comparison with the adiabatic energy difference $E_{AD}(2A_g^-) = E(2A_g^-$ at $2A_g^-$ minimum$) - E(1A_g^-$ at $1A_g^-$ minimum$)$ = 2.43 eV at SS-CASPT2/ANO-s level indicates an overestimation of ∼0.23 eV. For what concerns the $1A_g^- \rightarrow 1B_u^+$ transition, in the SI we estimate that E_{00} is in the energy region 2.65−2.75 eV. Therefore, comparison with the adiabatic energy difference $E_{AD}(1B_u^+) = E(1B_u^+$ at $1B_u^+$ minimum$) - E(1A_g^-$ at $1A_g^-$ minimum$)$ = 2.87 eV at SS-CASPT2/ANO-s level suggests an overestimation of 0.1−0.2 eV.

In conclusion, the absolute errors of the $2A_g^-$ and $1B_u^+$ energies in their minima are limited, being within 0.25 eV, and the inaccuracy on their relative stability is definitely smaller. The better performance of our CASPT2 approach in the excited-state minima with respect to the FC point is probably connected with the smaller interstate coupling. These results make us confident of the possibility of using our data for the qualitative discussion of the decay mechanism proposed in the following sections.

3.2.4. Paths Involving Torsional Distortions. The experimental results presented so far indicate that in chloroform a spectral evolution takes place on a time scale of 3−4 ps, leading to the intensification of an excited state absorption band at 1685 cm^{-1}. We interpret this band as a marker signature for the presence of an extra state in the deactivation path, which should thus be the ICT state. One possible interpretation of the observed dynamic evolution is the occurrence of a conformational variation in the system, leading to the stabilization of the ICT state. With the intent of exploring which molecular degree of freedom could have a substantial importance in the photodynamics, we analyzed what happens in case of distortions along torsional coordinates, which, inducing a

dx.doi.org/10.1021/jp505473j | J. Phys. Chem. B 2014, 118, 9613−9630

different stabilization or destabilization for each electronic state, lead to crossing of the PESs. Unfortunately, the computation of CASPT2 relaxed scans along each of the torsional degrees of freedom in 12-apocarotenal is unfeasible. On the other hand, it is experimentally known that 12-apocarotenal photoisomerizes (37.2% quantum yield) around the C13−C14 bond in acetonitrile.[66] On this ground we performed a rigid scan along the C13−C14 θ twisting coordinate at the MS-CASPT2//CASSF level, freezing all the other coordinates at the values they have in the $2A_g^-$ equilibrium geometry. The MOs of the active space change with θ, making it difficult to trace back the "diabatic character" of each adiabatic state. However, by using the MOs of the previous point as a guess for the next one, it is possible to follow the main CSFs of each state. The continuous lines in Figure 10 represent the MS-CASPT2 adiabatic energies along the path. At small torsional angles, the states can still be described and ordered as it was done at the FC point, while at θ = 20° they start to mix. We started the analysis by considering the GS($1A_g^-$), $2A_g^-$, $1B_u^+$, and $1B_u^-$ adiabatic states at their own equilibrium geometries as our reference "diabatic states" (and we label them $1A_g^-$, $2A_g^-$, $1B_u^+$, and $1B_u^-$, respectively). At each point of the path, we analyzed the similarity of the adiabatic states to the reference diabatic states comparing their composition in terms of CSFs (see Figure SI8). In particular, the dashed straight lines connect the states at θ = 0 and 90° that share the same "diabatic" character and provide a qualitative understanding of the crossings of the diabatic PESs along the path. Interestingly, Figure 10 shows that the $1B_u^+$ CSFs become more stable at the increase of θ, while the opposite occurs for the CFSs mainly contributing to $1A_g^-$ and $2A_g^-$ states. The coupling of the $1A_g^-$ and $1B_u^+$ becomes appreciable at θ = 45°; between θ = 40 and 60°, all the diabatic states are strongly coupled.

Such analysis witnesses that a crossing takes place between $2A_g^-$ and $1B_u^+$ at a small torsion angle (about 20−30 degrees of torsion), making the lowest excited state S_1 predominantly characterized by the $1Bu^+$ "diabatic" state. At the increase of θ we observe also a strong increase of the electric dipole moment and a simultaneous decrease of the oscillator strength for the S_1 state. The slightly activated rotation of 20−30° along the torsional coordinate could account for the 3−4 ps dynamic component observed in the experiments performed in chloroform, thus, rationalizing the spectral changes observed on this time scale. Notice that we reported MS-CASPT2 energies only, because rotation along θ induces a drastic mixing of the CASSCF wave functions so that SS-CASPT2 is not adequate. We remind that although MS-CASPT2 energies show a larger error for $2A_g^-$ at the FC point, they are very accurate and exhibit the same quality of SS-CASPT2 energies at the $2A_g^-$ minimum, the starting point of the path. Due to the computational cost of the calculations, we also adopted the smaller 6-31G(d) basis set; this leads to a destabilization of both $2A_g^-$ (0.3 eV) and $1B_u^+$ (0.14 eV), slightly decreasing their energy gap (by ∼0.15 eV). However, since for large distortions along θ, the $1B_u^+$ diabatic state correlates with the ground-state, the prediction that a crossing occurs between $2A_g^-$ and $1B_u^+$ remains valid.

The torsion along C13−C14 bond is not the only one distortion that can induce a crossing between $2A_g^-$ and $1B_u^+$ states. Preliminary scans at TD-DFT level actually suggest that this might happen twisting any of the C−C bonds where the LUMO orbital exhibits an antibonding character (see Supporting Information for further details). In particular, since C11−C12 photoisomerization has been extensively studied in retinoids, we computed a rigid scan at MS-CASPT2 level also along this torsion, finding a scenario very similar to that reported in Figure 10 (see Figure SI7)

3.2.5. Harmonic Vibrational Frequencies of Ground and Excited States. We computed numerically GS, $2A_g^-$ and $1B_u^+$ harmonic frequencies of two modes monitored by TD1-IR and TD2-IR spectra, namely the localized C═O stretching mode and a C═C symmetric mode. This latter is one of the most IR intense bands in the GS and the most coupled to the GS → $1B_u^+$ transition (i.e., the one showing the largest dimensionless displacement and hence one of the strongest FC progression, see Figure SI11, SI12).

At the $2A_g^-$ minimum, the C═C and C═O modes show a frequency upshift of 180 $cm^{-1}$and a down shift of −50 cm^{-1}, respectively, with respect to their GS values (namely, 1736, and 2001 cm^{-1}). On the other hand, in the $1B_u^+$ state the C═C and C═O frequencies upshift by 50 cm^{-1} and downshift by 120 cm^{-1}, respectively (see Table SI12). In summary, we predict a downshift of the C═O frequency larger in $1B_u^+$ and smaller in $2A_g^-$ and an upshift of the C═C frequency in both the excited states, but larger in $2A_g^-$.

3.3. Assignment of the Experimental IR Frequencies. The assignment of the GS vibrational spectrum of *trans-β*-apo-8′-carotenal in chloroform in the region 1500−1700 cm^{-1} is well established:[31] in this region, two bands at 1523 and 1660 cm^{-1} are of special interest, assigned to a symmetric C═C and to C═O stretching, respectively. These frequencies shift to 1530 and 1680 cm^{-1} in cyclohexane. Other resonances at 1565 and 1607 cm^{-1} in chloroform (1572 and 1615 cm^{-1} in cyclohexane) are due to asymmetric C═C stretching vibrations[31] (see FTIR spectra in chloroform and cyclohexane in SI).

The T1D-IR obtained in cyclohexane shows some negative bands, corresponding to ground state modes. We recognize one bleaching band around 1680 cm^{-1}, assigned to the C═O stretching, one at 1525 cm^{-1}, due to symmetric C═C stretching, and a very weak negative band at 1580 cm^{-1}, due to the C═C asymmetric stretching.

The assignment is definitely less obvious for the vibrations of the excited states in the 1600−1800 cm^{-1} region; nevertheless, an assignment has been proposed previously in the literature.[31]

As a matter of fact, it is well-known that the symmetric C═C stretching of polyenes in the S_1 excited state is shifted to a much higher frequency with respect to the ground state. The effect is due to the strong vibronic coupling of S_0 and S_1 states involving the totally symmetric vibrational mode.[78,79] This feature, common to a large family of conjugated chain molecules, is confirmed for *trans-β*-apo-12′-carotenal by our CASSCF computations, which predict an upshift of ∼180 cm^{-1} of the C═C stretching in the $2A_g^-$ minimum. On this ground, we can assign the intense absorption band observed in cyclohexane at 1750 cm^{-1} in the second and third EADS (blue and red lines in Figure 3A) to the symmetric C═C stretching of the $2A_g^-$ excited state. In fact, the experimental upshift of ∼220 cm^{-1} nicely matches the computed value (∼180 cm^{-1}). On the same base, the band at ∼1600 cm^{-1}can be assigned to the C═O stretching, after noticing that its downshift (∼−80 cm^{-1}) is in line with the computed value in the gas phase (∼−50 cm^{-1}).

In chloroform the absorption bands look different, being much broader, with a rather complex profile; it is difficult to disentangle bands pertaining to specific modes. However,

dx.doi.org/10.1021/jp505473j | J. Phys. Chem. B 2014, 118, 9613−9630

analogies with the corresponding spectrum in cyclohexane, together with the observation that the vibrational frequencies, as a general trend, downshift as the solvent polarity increases, may help in the assignment. First, the band at ∼1590 cm^{-1}, being slightly lower than in cyclohexane (the shift is −10 cm^{-1}, to be compared to the −20 cm^{-1} red-shift in the GS), can be safely assigned to the excited state C=O stretching. Our computations suggest that the $1B_u^+$ and $2A_g^-$ frequencies should be very similar so that they might not be distinguishable. Moreover, it is reasonable to assume that the two bands at 1685 and 1715 cm^{-1} are both associated with the symmetric C=C since, as discussed above, it has the unique characteristic to be upshifted in both $2A_g^-$ and $1B_u^+$. In this sense, the highest value (1715 cm^{-1}), being up-shifted by ∼190 cm^{-1} with respect to the GS value (1523 cm^{-1}), is more compatible with a mode of the $2A_g^-$ state.

4. DISCUSSION

We can now propose a general picture of the decay mechanism of photoexcited 8-carotenal and of its dependence on the solvent, based on the experimental observations and the computational results reported in the previous sections, together with what is known from the literature on analogous systems. The energy profiles in Figure 9 suggest that, after photoexcitation to the $1B_u^+$ excited state, the system evolves via a conical intersection to the $2A_g^-$ minimum. This process can be associated with the ultrafast decay (ca. 200 fs) deduced from EADS analysis. In this sense, the bands at 1710 (cyclohexane) and 1680 cm^{-1} (chloroform) observed in the first EADS (black line in Figure 2A and B, respectively) are assigned to the C=C band in the $1B_u^+$ state. In their time evolution, these bands shift to 1750 cm^{-1} (cyclohexane, Figure 2A) and 1715 cm^{-1} (chloroform, Figure 2B), respectively, thus signaling the rise of the $2A_g^-$ population.

Once the S_1 ($2A_g^-$) minimum is populated, the system can further evolve along competing radiative and nonradiative channels. Actually, the $2A_g^-$ minimum exhibits small oscillator strength, nonetheless it might give rise to a detectable emission if it survives for a sufficient time. Indeed, weak fluorescence has been measured for carbonyl carotenoids,[16,80] and a recent study reports on time-resolved fluorescence measurements on peridinin and several molecular analogues.[81]

The radiationless deactivation to the GS state proceeds either through a direct $2A_g^- \rightarrow$ GS decay or through an intermediate excited-state. In terms of the structural distortions involved in the process, chemical intuition and literature data on similar systems suggest two possible radiationless deactivation paths that involve (a) out of plane C−C torsional distortions[66] (similar to retinal[82]) and (b) in-plane change of the C−C bond length alternation.[83]

The S_1 decay constant of unsubstituted carotenoids does not exhibit solvent dependence, because it depends primarily on the conjugation length and nicely correlates with the $E(2A_g^-) - E(GS)$ energy gap.[13] The same trend is observed for carbonyl-substituted carotenoids in nonpolar solvents.[16] Furthermore, a study on all-*trans*-β-carotene shows that vibronic coupling through the in-phase C−C BLA mode plays a major role in the $2A_g^- \rightarrow$ GS internal conversion.[83]

As far as our data in cyclohexane are concerned, there is no evidence of any involvement of a further electronic state, since the only spectral evolution after formation of $2A_g^-$ is a slight blue shift of the 1750 cm^{-1} band, which is fully compatible with vibrational cooling in the $2A_g^-$ potential well. Therefore, we can conclude that in cyclohexane $2A_g^-$ decays directly to GS, a process that according to the above discussion should be enhanced by a motion along the BLA vibration.[83]

In chloroform, experimental results show a reduction of the lifetime of the S_1 state together with a red−blue−red evolution in time of the C=C excited-state frequency. This behavior reveals significant changes of the electronic structure in polar solvents. More generally, the same simple mechanism acting in cyclohexane does not appear to be compatible with the decay in chloroform. In fact, T2D-IR in chloroform recorded 3 ps after the electronic excitation shows that the observed TD1-IR broad band in the C=C stretching region is related to two peaks with different rise times, as observed from the kinetic traces reported in Figures 4 and 7, and this calls for the involvement of an additional excited state beyond $2A_g^-$.

As solvent polarity mainly affects states with large electric dipole, there is a general consensus on the fact that the new state involved in chloroform has a partial ICT character. Recent studies suggest that that ICT arises from a solvent induced mixing of the $2A_g^-$ and $1B_u^+$ states and is close in energy with these two low lying excited states.[20,84]

According to our calculations, the $1B_u^+$ state has several characteristics which make it a suitable candidate for the ICT role. Actually, it exhibits (a) a low-energy, with respect to carotenes (see section 5 in the SI and refs 13 and 51) caused by the carbonyl substitution, (b) an electron density transfer from one part to the other of the molecule, (c) a high electric dipole moment, and (d) a stabilization in polar solvents in equilibrium and nonequilibrium regimes, both for 12-apocarotenal and 8-apocarotenal. Moreover, according to our multireference calculations, no other state with large electric dipole is predicted among the lowest-excited states at any of the minima of the GS, $2A_g^-$ and $1B_u^+$ states.

Our experimental and computational evidence therefore indicate that the $1B_u^+$ state is the dominant contributor to the ICT state (the others being the $2A_g^-$ and GS diabatic states, see Figure 10).

However, it remains to be clarified how it is repopulated starting from the $2A_g^-$ minimum. Such a process cannot be simply driven by a solvent reorganization, since solvent would rearrange in order to stabilize the populated state ($2A_g^-$), thus, lowering its energy with respect to $1B_u^+$. Therefore, a molecular distortion is needed to trigger this process, and according to our MS-CASPT2 energy profiles in Figure 10, the rotation along θ is a very good candidate.

This idea agrees with recent time-resolved measurements performed on peridinin and other similar molecules, in the visible and near-infrared range. In this spectral region, stimulated emission (SE) features attributed to ICT were detected in polar solvents.[81] The authors observe that, in principle, SE is permitted only for optically allowed transitions, but $1B_u^+$ spontaneous fluorescence and direct $S_0 \rightarrow 1B_u^+$ absorption are not observed. This implies that ICT is not accessible through vertical transition, so that ICT stimulated emission occurs after a substantial molecular rearrangement.

Our hypothesis is that, in polar solvents, once the $2A_g^-$ minimum is populated, a small distortion along the θ twist on the $2A_g^-$ PES brings the $1B_u^+$ and $2A_g^-$ states close enough to permit a $2A_g^- \rightarrow 1B_u^+$ back-transfer. Once back on the $1B_u^+$, the system quickly abandons the $2A_g^-/1B_u^+$ interaction region, as the energy gradient drives it in toward the region $\theta = 90°$ and solvent equilibration progressively stabilizes $1B_u^+$ with respect to $2A_g^-$. The experimental time constant of 3−4 ps,

dx.doi.org/10.1021/jp505473j | J. Phys. Chem. B 2014, 118, 9613−9630

corresponding to the decay of the second EADS and to the rising time of the 1685 cm^{-1} band in the kinetic traces in Figures 4 and 7, is in a reasonable time scale for this (slightly) activated process.

In section 3.1.3 we noticed that the off-diagonal peaks, measured in the C=C stretching region of the T2D-IR map, connect that vibration in $2A_g^-$ state the to the same mode vibrating in the $1B_u^+$ state, showing the same rise time (3.7 ps) of the latter. We emphasize here that this spectral feature represents the most direct experimental evidence for the proposed population transfer between $2A_g^-$ and $1B_u^+$.

The proposed mechanism is supported by the MS-CASPT2 energy profiles shown in Figure 10 for 12-apocarotenal in the gas-phase. 8-apocarotenal in polar solution is expected to exhibit a similar scenario; in fact, the increased stabilization of the $2A_g^-$ state due to the longer chain-length (Table 1) should be roughly balanced by the stabilization of the $1B_u^+$ state in a polar solvent (Table 3). The proposed $1B_u^+ \rightarrow 2A_g^- \rightarrow 1B_u^+ \rightarrow$ GS mechanism provides a natural explanation for the observation that in chloroform the C=C stretching frequency in the excited-state first blue-shifts (first → second EADS) and then red-shifts back (second → third EADS), thus, recovering at longer delay times the value it exhibits right after the photoexcitation. Moving from chloroform to cyclohexane, $1B_u^+$ becomes less stable and larger distortions along θ are required on the $2A_g^-$ PES to recover the increased $E(1B_u^+) - E(2A_g^-)$ energy gap at the $2A_g^-$ minimum. This is unlikely since such distortions are energetically costly on the $2A_g^-$ PES, and this explains why in this solvent the ICT state is not involved in the decay. Therefore, in our hypothesis, what makes the difference between the dynamics in nonpolar and polar solvents is not the behavior on the $2A_g^-$ state, whose PES is only slightly affected by the solvent polarity, but the fact that in polar solvents $1B_u^+$ is more stable. The result is that smaller rotations along θ are necessary to bring $1B_u^+$ and $2A_g^-$ close together and allow the population transfer.

On the same foot, our proposed mechanism can also suggest why in long chain apocarotenals[16] the excited-state lifetime does not strongly decrease with the increase of the solvent polarity: in those systems, in fact, the increased stability of the $2A_g^-$ state makes the $2A_g^- \rightarrow 1B_u^+$ back-transfer more difficult, while it favors the direct $2A_g^- \rightarrow 1A_g^-$ decay. Previous transient-absorption measurements suggest that the ICT state is populated also in nonpolar solvents in both 12-apocarotenal[17] and 8-apocarotenal,[16] but that the ICT bands are more intense in 12-apocarotenal.[17] Our results suggest that, if a ICT population is formed in 8-apocarotenal in cyclohexane, it is too small to be evidenced by our measurements. In any case, even the observations in refs 16, 17, and 51 can fit with the scenario reported in Figure 10 and described above, since (i) both $2A_g^-$ and $1B_u^+$ state exhibit similar stability, (ii) as shown in Table 1, sixth column, the $1B_u^+$ state is more stabilized with respect to $2A_g^-$ in 12-apocarotenal than in 8-apocarotenal, a fact that should favor ICT population.

We believe that all the experimental observations reported in our work can be rationalized within the mechanism we propose on the basis of the computational analysis. However, it should be emphasized that the interplay among the different factors playing a role in the process, namely, the states' stabilities, their dependence on the chain length, the solvent static and dynamic effects, is definitely very delicate, so that no state-of-the art computational model is expected to give a quantitative account for all the experimental data.

In section 3.2.3 we analyzed the reliability of our calculations, showing that they are quite accurate in the region of the $1B_u^+$ and $2A_g^-$ and minima, an important aspect since the mechanism we propose for the repopulation of $1B_u^+$ starts from the $2A_g^-$ minimum. The error is on the contrary sensibly larger at the FC point, especially for the overestimation of the $2A_g^-$ energy; so that in reality $2A_g^-$ is likely as stable as, or even more stable than, $1B_u^+$. The prediction that the two states are coupled in the FC region, as well as the fact that $2A_g^-$ is the lowest excited state in the $1B_u^+$ minimum, are however in line with the ultrafast decay of the initially excited $1B_u^+$ toward $2A_g^-$, a phenomenon that is well established experimentally and confirmed by our observations (<200 fs).

The S_1 adiabatic energy reported in Figure 10 slightly increases with θ. While the rather long relaxation times to GS are compatible with the existence of local minima on the S_1 state,[29] the large energy gap we predict between S_1 and S_0 is clearly biased by the fact that all the geometrical parameters, except θ, are frozen at the $2A_g^-$ minimum, and the solvent effect is not considered. Accounting for these effects would allow the S_1 PES to get much closer to the S_0 one, in line with the fact that photoisomerization is indeed possible and it has been observed in acetonitrile, even if with a moderate yield.[66]

It is interesting to notice that, if structural and solvent relaxations allow the system to undergo large distortion along θ, according to our calculations (see Figures 10 and SI8 in the Supporting Information), the S_1 state gains a remarkable component from the $1A_g^-$ diabatic state. This results in an even larger charge transfer character (the electric dipole increases from ∼14 to ∼30 D when θ goes from 40 to 90°, Figure 10). The very suggestive hypothesis that the $1A_g^-$ configuration (i.e., the GS state at the FC geometry) contributes together with $1B_u^+$ to the formation of the ICT state might be verified only by a nonadiabatic dynamical simulation including solvent relaxation effects.

In the previous discussion we did not consider either the possible role in the decay process of the $1B_u^-$ state, or other solvent properties, such as polarizability, which could also play a role in stabilizing the ICT state. Concerning the involvement of $1B_u^-$, our calculations predict that in the FC region it lies well above the photoexcited $1B_u^+$ state. According to some theoretical and experimental papers on linear polyenes, $1B_u^-$ becomes more stable than $1B_u^+$ for long chains, the inversion threshold being around a number of double-bonds $N = 8$.[76] Carotenals are not expected to follow exactly the same energy order as linear polyenes, and in SI we show that the relative stability of $1B_u^+$ over $1B_u^-$ increases by ∼0.15 eV in 12-apocarotenal with respect to 12-carotene. Additionally, a recent DFT/MRCI study on the carotenal peridinin indicates that $1B_u^-$ does not contribute to the two lowest excited adiabatic states S_1 and S_2, even for large variations of the BLA coordinate.[71] Besides these important differences, the possibility that even in the investigated carotenals $1B_u^-$ exhibits a minimum with energies comparable to $1B_u^+$ in the gas phase does not contradict the mechanism we propose. In fact, the dynamic behavior of the system initially excited to the $1B_u^+$ state is mostly determined by the relative stabilities of the different states along the path from the FC region toward the $1B_u^+$ minimum. Our calculations in the gas phase suggest that $1B_u^-$ remains at definitely higher energies, so that no exchange of population is foreseen. In polar solvents, the stabilization of $1B_u^+$ over $1B_u^-$ is expected to increase.

dx.doi.org/10.1021/jp505473j | J. Phys. Chem. B 2014, 118, 9613−9630

In summary, while we cannot completely exclude that the $1B_u^-$ state takes part in the decay of 12-apocarotenal and 8-apocarotenal in nonpolar and polar solution, neither our experimental nor our computational results point out any clear mark of its involvement.

5. CONCLUSIONS

Time-resolved IR measurements on 8-carotenal performed both in cyclohexane and chloroform evidenced several interesting features:

(1) Transient infrared spectra in polar and nonpolar solvents are very different: broad positive bands are observed in chloroform, while sharp bleaching and excited state absorption bands can be distinguished in cyclohexane.
(2) While in cyclohexane the dynamic evolution of the IR spectra on a 3−4 ps time scale can be interpreted in terms of vibrational relaxation, a more complex behavior is evidenced in chloroform, where the band at 1685 cm^{-1} shows a rise component on this time scale.
(3) In chloroform, the excited-state C═C stretching frequency blue-shifts (1680 → 1715 cm^{-1}) and then red-shifts again in time, recovering the initial value assumed immediately after the photoexcitation.
(4) T2D-IR spectra allowed to clearly identify a double band structure in the 1680−1750 cm^{-1} spectral region in chloroform and a cross peak connecting these two resonances. The kinetic behavior of these two peaks coincide with that obtained with the T1D-IR experiment, confirming that the peak at 1685 cm^{-1} has a rise component on a 3−4 ps time scale. The cross peak has the same rise time of the ∼1680 cm^{-1} diagonal band.

Based on this experimental information and on a detailed theoretical analysis of the energies, electronic structure, vibrational frequencies, and potential energy surfaces of the low lying excited states of 8-carotenal, we propose a deactivation mechanism for this molecule and elucidate the nature of the ICT state. According to our interpretation, radiationless decay in carbonyl carotenoids proceeds primarily via conical intersection between the initially populated $1B_u^+$ state and the symmetry forbidden $2A_g^-$ state. The involvement of a further excited state with ICT character in the deactivation path has been invoked in the literature. We propose that the bright $1B_u^+$ state is the main contributor to the ICT state, and that in polar solvents it is repopulated via a slightly activated mechanism proceeding through a molecular distortion involving the rotation around a C−C bond from the $2A_g^-$ minimum. The repopulation of the $1B_u^+$ diabatic state shortens the GS recovery time for two main reasons: (i) this diabatic state is strongly stabilized through the torsion θ and is directly correlated with the adiabatic GS at $\theta = 90°$ (Figure 10); (ii) the solvent equilibration further stabilizes this state (by at least 0.12 eV in chloroform, and by more than 0.3 eV in methanol).

In summary, our study indicates that no other excited diabatic state beyond $1B_u^+$ and $2A_g^-$ plays a significant role in the decay of 8-apocarotenal, and that $1B_u^+$ is the main contributor to the ICT state observed in polar solvents, thus, supporting what we named "the two-state model" in the Introduction. Moreover, it suggests that, if solvent relaxation makes large distortions along the chain twisting coordinate energetically favorable, the ICT state may acquire also a contribution from the diabatic state $1A_g^-$ corresponding to the ground-state at the Franck−Condon geometry.

As we pointed out in the Introduction, because of the length of the polyene chain of 8-apocarotenal, the $2A_g^-$ and $1B_u^+$ states lie close in energy and can interact in a large region of the nuclear configurations. Due to this peculiarity, our results provide some hints to rationalize the behavior of short and long-chain carotenoids. We showed that, at the increase of the chain length, $2A_g^-$ is progressively stabilized with respect both to $1B_u^+$ state and, even more, to GS state (Table 1). In carotenoids longer than 8-apocarotenal, these facts favor the direct decay to GS (that becomes faster according to the energy-gap rule) with respect to the $2A_g^- \rightarrow 1B_u^+$ back transfer. As a consequence, in these systems the excited-state lifetime becomes shorter at the increase of the chain length because of the remarkable stabilization of $2A_g^-$ with respect to GS, but it does not decrease at the increase of the polarity of the solvent,[16] since the ICT state does not play a relevant role in the decay. On the contrary, in shorter carotenoids, $1B_u^+$ state is stabilized with respect to $2A_g^-$, favoring the formation of the ICT state: this latter has indeed been observed for 12-apocarotenal also in nonpolar solvents. In retinal, in agreement with previous results,[82] our SS-CASPT2 computations predict that at the FC point the $2A_g^-$ is ∼0.18 eV less stable than $1B_u^+$ (Table SI5, Supporting Information). Since the $2A_g^-$ gradient is larger than the $1B_u^+$ one (Figure 9), it is reasonable that the former state acts as an intermediate state in the decay, in agreement with the common interpretations reported in literature.[51] The peculiarity of retinal is the involvement in the decay in nonpolar solvents of a low-lying $n\pi^*$ state that is too unstable to play a role in longer carotenoids (see Table SI1 in Supporting Information). However, in methanol, polarity and hydrogen bonding lead to a remarkable (relative) destabilization of the $n\pi^*$ state with respect to the $1B_u^+$ state; this accounts for the possible formation of an ICT state, as recently confirmed by experiments.[51]

■ ASSOCIATED CONTENT

Supporting Information

Detailed computational information; Nature of excited states in FC region; Equilibrium geometries; Paths involving torsion distortions; Harmonic vibrational frequencies of ground and excited states; Experimental and theoretical FTIR and UV/vis Spectra; Broadband Transient IR/IR spectra; T2D-IR maps recorded at different vis-pump/IR-probe delay; Vertical energies for retinal. This material is available free of charge via the Internet at http://pubs.acs.org.

■ AUTHOR INFORMATION

Corresponding Authors

*E-mail: lapini@lens.unifi.it.
*E-mail: fabrizio.santoro@iccom.cnr.it.

Author Contributions

†These authors have equally contributed to this work (M.D.D. and M.S.C.).

Notes

The authors declare no competing financial interest.

■ ACKNOWLEDGMENTS

The authors acknowledge the Italian "Ministero dell'Istruzione dell'Università e della Ricerca' (FIRB "Futuro in Ricerca" 2010, RBFR10Y5VW to M.D.D. and C.C.; PRIN 2010-2011 2010ERFKXL "Frontiers studies in molecular spectroscopy and dynamics: from simple molecular systems to supra-

molecular aggregates and advanced materials" to F.S. and R.R.). A.L. acknowledges the financial support of the Regione Toscana through the found POR-FSE 2007-2013 obiettivo 2 asse IV, Project EPHODS. F.A. acknowledges support from EU People Program, Marie Curie Actions (G.A. No. 246550). The financial support of the Cassa di Risparmio di Firenze is also gratefully acknowledged. C.C. acknowledges support from COST (Action CODECS: COnvergent Distributed Environment for Computational Spectroscopy). The authors thank R. Improta (IBB-CNR, Napoli) and C. Angeli (University of Ferrara) for fruitful discussions.

REFERENCES

(1) Frank, H. A.; Cogdell, R. J. Carotenoids in Photosynthesis. *Photochem. Photobiol.* **1996**, *63*, 257−264.

(2) Ostroumov, E. E.; Mulvaney, R. M.; Cogdell, R. J.; Scholes, G. D. Broadband 2D Electronic Spectroscopy Reveals a Carotenoid Dark State in Purple Bacteria. *Science* **2013**, *340*, 52−56.

(3) van Amerongen, H.; van Grondelle, R. Understanding the Energy Transfer Function of LHCII, the Major Light-Harvesting Complex of Green Plants. *J. Phys. Chem. B* **2000**, *105*, 604−617.

(4) Demmig-Adams, B.; Adams, W. W. Photosynthesis: Harvesting Sunlight Safely. *Nature* **2000**, *403*, 371−374.

(5) Niyogi, K. K. Photoprotection Revisited: Genetic and Molecular Approaches. *Annu. Rev. Plant Physiol. Plant Mol. Biol.* **1999**, *50*, 333−359.

(6) Edge, R.; McGarvey, D. J.; Truscott, T. G. The Carotenoids as Anti-Oxidants: a Review. *J. Photochem. Photobiol., B* **1997**, *41*, 189−200.

(7) Liu, L.; Zhan, W. Molecular Photovoltaic System Based on Fullerenes and Carotenoids Co-assembled in Lipid/Alkanethiol Hybrid Bilayers. *Langmuir* **2012**, *28*, 4877−4882.

(8) Maiuri, M.; Snellenburg, J. J.; van Stokkum, I. H. M.; Pillai, S.; WongCarter, K.; Gust, D.; Moore, T. A.; Moore, A. L.; van Grondelle, R.; Cerullo, G.; et al. Ultrafast Energy Transfer and Excited State Coupling in an Artificial Photosynthetic Antenna. *J. Phys. Chem. B* **2013**, *117*, 14183−14190.

(9) Pillai, S.; Ravensbergen, J.; Antoniuk-Pablant, A.; Sherman, B. D.; van Grondelle, R.; Frese, R. N.; Moore, T. A.; Gust, D.; Moore, A. L.; Kennis, J. T. M. Carotenoids as Electron or Excited-state Energy Donors in Artificial Photosynthesis: an Ultrafast Investigation of a Carotenoporphyrin and a Carotenofullerene Dyad. *Phys. Chem. Chem. Phys.* **2013**, *15*, 4775−4784.

(10) Cerullo, G.; Polli, D.; Lanzani, G.; De Silvestri, S.; Hashimoto, H.; Cogdell, R. J. Photosynthetic Light Harvesting by Carotenoids: Detection of an Intermediate Excited State. *Science* **2002**, *298*, 2395−2398.

(11) Gradinaru, C. C.; Kennis, J. T. M.; Papagiannakis, E.; van Stokkum, I. H. M.; Cogdell, R. J.; Fleming, G. R.; Niederman, R. A.; van Grondelle, R. An unusual Pathway of Excitation Energy Deactivation in Carotenoids: Singlet-to-Triplet Conversion on an Ultrafast Timescale in a Photosynthetic Antenna. *Proc. Natl. Acad. Sci. U.S.A.* **2001**, *98*, 2364−2369.

(12) Paulsen, H. *The Photochemistry of Carotenoids*; Kluwer Academic Publisher: Dordrecht, 1999; pp 123−135.

(13) Polivka, T.; Sundström, V. Ultrafast Dynamics of Carotenoid Excited States. From Solution to Natural and Artificial Systems. *Chem. Rev.* **2004**, *104*, 2021−2072.

(14) Orlandi, G.; Zerbetto, F.; Zgierski, M. Z. Theoretical Analysis of Spectra of Short Polyenes. *Chem. Rev.* **1991**, *91*, 867−891.

(15) Tavan, P.; Schulten, K. Electronic Excitations in Finite and Infinite Polyenes. *Phys. Rev. B* **1987**, *36*, 4337−4358.

(16) Ehlers, F.; Wild, D. A.; Lenzer, T.; Oum, K. Investigation of the S1/ICT→ S0 Internal Conversion Lifetime of 4′-Apo-β-caroten-4′-al and 8′-Apo-β-caroten-8′-al: Dependence on Conjugation Length and Solvent Polarity. *J. Phys. Chem. A* **2007**, *111*, 2257−2265.

(17) Kopczynski, M.; Ehlers, F.; Lenzer, T.; Oum, K. Evidence for an Intramolecular Charge Transfer State in 12′-Apo-β-caroten-12′-al and 8′-Apo-β-caroten-8′-al: Influence of Solvent Polarity and Temperature. *J. Phys. Chem. A* **2007**, *111*, 5370−5381.

(18) Wild, D. A.; Winkler, K.; Stalke, S.; Oum, K.; Lenzer, T. Extremely Strong Solvent Dependence of the S1 → S0 Internal Conversion Lifetime of 12′-Apo-β-caroten-12′-al. *Phys. Chem. Chem. Phys.* **2006**, *8*, 2499−2505.

(19) Zigmantas, D.; Hiller, R. G.; Yartsev, A.; Sundström, V.; Polivka, T. Dynamics of Excited States of the Carotenoid Peridinin in Polar Solvents: Dependence on Excitation Wavelength, Viscosity, and Temperature. *J. Phys. Chem. B* **2003**, *107*, 5339−5348.

(20) Enriquez, M. M.; Fuciman, M.; LaFountain, A. M.; Wagner, N. L.; Birge, R. R.; Frank, H. A. The Intramolecular Charge Transfer State in Carbonyl-Containing Polyenes and Carotenoids. *J. Phys. Chem. B* **2010**, *114*, 12416−12426.

(21) Papagiannakis, E.; Vengris, M.; Larsen, D. S.; van Stokkum, I. H. M.; Hiller, R. G.; van Grondelle, R. Use of Ultrafast Dispersed Pump-Dump-Probe and Pump-Repump-Probe Spectroscopies to Explore the Light-Induced Dynamics of Peridinin in Solution. *J. Phys. Chem. B* **2005**, *110*, 512−521.

(22) Bonetti, C.; Alexandre, M. T. A.; van Stokkum, I. H. M.; Hiller, R. G.; Groot, M. L.; van Grondelle, R.; Kennis, J. T. M. Identification of Excited-State Energy Transfer and Relaxation Pathways in the Peridinin-Chlorophyll Complex: an Ultrafast Mid-Infrared Study. *Phys. Chem. Chem. Phys.* **2010**, *12*, 9256−9266.

(23) Papagiannakis, E.; van Stokkum, I. H. M.; Vengris, M.; Cogdell, R. J.; van Grondelle, R.; Larsen, D. S. Excited-State Dynamics of Carotenoids in Light-Harvesting Complexes. 1. Exploring the Relationship between the S1 and S* States. *J. Phys. Chem. B* **2006**, *110*, 5727−5736.

(24) Shima, S.; Ilagan, R. P.; Gillespie, N.; Sommer, B. J.; Hiller, R. G.; Sharples, F. P.; Frank, H. A.; Birge, R. R. Two-Photon and Fluorescence Spectroscopy and the Effect of Environment on the Photochemical Properties of Peridinin in Solution and in the Peridinin-Chlorophyll-Protein from Amphidinium carterae. *J. Phys. Chem. A* **2003**, *107*, 8052−8066.

(25) Vaswani, H. M.; Hsu, C.-P.; Head-Gordon, M.; Fleming, G. R. Quantum Chemical Evidence for an Intramolecular Charge-Transfer State in the Carotenoid Peridinin of Peridinin-Chlorophyll-Protein. *J. Phys. Chem. B* **2003**, *107*, 7940−7946.

(26) Durchan, M.; Fuciman, M.; Šlouf, V.; Kesan, G.; Polivka, T. Excited-State Dynamics of Monomeric and Aggregated Carotenoid 8′-Apo-β-carotenal. *J. Phys. Chem. A* **2012**, *116*, 12330−12338.

(27) Zigmantas, D.; Hiller, R. G.; Sundström, V.; Polivka, T. Carotenoid to Chlorophyll Energy Transfer in the Peridinin-Chlorophyll-Protein Complex Involves an Intramolecular Charge Transfer State. *Proc. Natl. Acad. Sci. U.S.A.* **2002**, *99*, 16760−16765.

(28) Gonzàlez-Luque, R.; Garavelli, M.; Bernardi, F.; Merchàn, M.; Robb, M. A.; Olivucci, M. Computational Evidence in Favor of a Two-State, Two-Mode Model of the Retinal Chromophore Photoisomerization. *Proc. Natl. Acad. Sci. U.S.A.* **2000**, *97*, 9379−9384.

(29) Pang, Y.; Fleming, G. R. Branching Relaxation Pathways from the Hot S2 State of 8′-Apo-β-caroten-8′-al. *Phys. Chem. Chem. Phys.* **2010**, *12*, 6782−6788.

(30) Pang, Y.; Jones, G. A.; Prantil, M. A.; Fleming, G. R. Unusual Relaxation Pathway from the Two-Photon Excited First Singlet State of Carotenoids. *J. Am. Chem. Soc.* **2010**, *132*, 2264−2273.

(31) Pang, Y.; Prantil, M. A.; Van Tassle, A. J.; Jones, G. A.; Fleming, G. R. Excited-State Dynamics of 8′-Apo-β-caroten-8′-al and 7′,7′-Dicyano-7′-apo-β-carotene Studied by Femtosecond Time-Resolved Infrared Spectroscopy. *J. Phys. Chem. B* **2009**, *113*, 13086−13095.

(32) Zanni, M. T.; Hamm, P. *Concepts and Methods of 2D Infrared Spectroscopy*; Cambridge University Press: New York, 2011.

(33) Bredenbeck, J.; Helbing, J.; Kolano, C.; Hamm, P. Ultrafast 2D−IR Spectroscopy of Transient Species. *ChemPhysChem* **2007**, *8*, 1747−1756.

(34) Santoro, F.; Lami, A.; Improta, R.; Barone, V. Effective Method to Compute Vibrationally Resolved Optical Spectra of Large Molecules at Finite Temperature in the Gas Phase and in Solution. *J. Chem. Phys.* **2007**, *126*, 184102.

(35) Park, S.; Kwak, K.; Fayer, M. D. Ultrafast 2D-IR Vibrational Echo Spectroscopy: a Probe of Molecular Dynamics. *Laser Phys. Lett.* **2007**, *4*, 704−718.
(36) Shim, S.-H.; Zanni, M. T. How to Turn Your Pump-Probe Instrument into a Multidimensional Spectrometer: 2D IR and Vis Spectroscopies via Pulse Shaping. *Phys. Chem. Chem. Phys.* **2009**, *11*, 748−761.
(37) Hendler, R. W.; Shrager, R. I. Deconvolutions Based on Singular Value Decomposition and the Pseudoinverse: a Guide for Beginners. *J. Biochem. Biophys. Meth.* **1994**, *28*, 1−33.
(38) Henry, E. R. The Use of Matrix Methods in the Modeling of Spectroscopic Data Sets. *Biophys. J.* **1997**, *72*, 652−673.
(39) Henry, E. R.; Hofrichter, J. Singular Value Decomposition: Application to Analysis of Experimental Data. In *Methods in Enzymology*, Ludwig Brand, M. L. J., Ed.; Academic Press: New York, 1992; Vol. *210*, pp 129−192.
(40) van Stokkum, I. H. M.; Larsen, D. S.; van Grondelle, R. Global and Target Analysis of Time-Resolved Spectra. *Biochim. Biophys. Acta, Bioenerg.* **2004**, *1657*, 82−104.
(41) Mullen, K. M.; van Stokkum, I. H. M. An Introduction to the Special Volume "Spectroscopy and Chemometrics in R. *J. Stat. Soft.* **2007**, *18*, 1−5.
(42) Snellenburg, J. J.; Laptenok, S. P.; Seger, R.; Mullen, K. M.; van Stokkum, I. H. M. Glotaran: A Java-Based Graphical User Interface for the R Package TIMP. *J. Stat. Soft.* **2012**, *49*, 1−22.
(43) Yanai, T.; Tew, D. P.; Handy, N. C. A New Hybrid Exchange−Correlation Functional Using the Coulomb-Attenuating Method (CAM-B3LYP). *Chem. Phys. Lett.* **2004**, *393*, 51−57.
(44) Roos, B. O. The Complete Active Space Self-Consistent Field Method and its Applications in Electronic Structure Calculations. In *Adv. Chem. Phys.*; John Wiley & Sons, Inc.: New York, 2007; pp 399−445.
(45) Scalmani, G.; Frisch, M. J.; Mennucci, B.; Tomasi, J.; Cammi, R.; Barone, V. Geometries and Properties of Excited States in the Gas Phase and in Solution: Theory and Application of a Time-Dependent Density Functional Theory Polarizable Continuum Model. *J. Chem. Phys.* **2006**, *124*, 094107.
(46) Andersson, K.; Malmqvist, P. A.; Roos, B. O.; Sadlej, A. J.; Wolinski, K. Second-Order Perturbation Theory with a CASSCF Reference Function. *J. Phys. Chem.* **1990**, *94*, 5483−5488.
(47) Finley, J.; Malmqvist, P.-Å.; Roos, B. O.; Serrano-Andrés, L. The Multi-State CASPT2Method. *Chem. Phys. Lett.* **1998**, *288*, 299−306.
(48) Valsson, O.; Angeli, C.; Filippi, C. Excitation Energies of Retinal Chromophores: Critical Role of the Structural Model. *Phys. Chem. Chem. Phys.* **2012**, *14*, 11015−11020.
(49) Frutos, L. M.; Andruniòw, T.; Santoro, F.; Ferré, N.; Olivucci, M. Tracking the Excited-State Time Evolution of the Visual Pigment with Multiconfigurational Quantum Chemistry. *Proc. Natl. Acad. Sci. U.S.A.* **2007**, *104*, 7764−7769.
(50) Schapiro, I.; Ryazantsev, M. N.; Frutos, L. M.; Ferré, N.; Lindh, R.; Olivucci, M. The Ultrafast Photoisomerizations of Rhodopsin and Bathorhodopsin are Modulated by Bond Length Alternation and HOOP Driven Electronic Effects. *J. Am. Chem. Soc.* **2011**, *133*, 3354−3364.
(51) Polivka, T.; Kaligotla, S.; Chabera, P.; Frank, H. A. An Intramolecular Charge Transfer State of Carbonyl Carotenoids: Implications for Excited State Dynamics of Apo-carotenals and Retinal. *Phys. Chem. Chem. Phys.* **2011**, *13*, 10787−10796.
(52) Roos, B. O.; Andersson, K. Multiconfigurational Perturbation Theory with Level Shift: the Cr_2 Potential Revisited. *Chem. Phys. Lett.* **1995**, *245*, 215−223.
(53) Malmqvist, P. Å. Calculation of Transition Density Matrices by Non-unitary Orbital Transformations. *Int. J. Quantum Chem.* **1986**, *30*, 479−494.
(54) Mennucci, B. Polarizable Continuum Model. *Wiley Interdiscip. Rev.: Comput. Mol. Sci.* **2012**, *2*, 386−404.
(55) Tomasi, J.; Mennucci, B.; Cammi, R. Quantum Mechanical Continuum Solvation Models. *Chem. Rev.* **2005**, *105*, 2999−3094.
(56) Cammi, R.; Corni, S.; Mennucci, B.; Tomasi, J. Electronic Excitation Energies of Molecules in Solution: State Specific and Linear Response Methods for Non-Equilibrium Continuum Solvation Models. *J. Chem. Phys.* **2005**, *122*, 104513.
(57) Corni, S.; Cammi, R.; Mennucci, B.; Tomasi, J. Electronic Excitation Energies of Molecules in Solution within Continuum Solvation Models: Investigating the Discrepancy between State-Specific and Linear-Response Methods. *J. Chem. Phys.* **2005**, *123*, 134512.
(58) Improta, R.; Barone, V.; Scalmani, G.; Frisch, M. J. A State-Specific Polarizable Continuum Model Time Dependent Density Functional Theory Method for Excited State Calculations in Solution. *J. Chem. Phys.* **2006**, *125*, 054103.
(59) Improta, R.; Scalmani, G.; Frisch, M. J.; Barone, V. Toward Effective and Reliable Fluorescence Energies in Solution by a New State Specific Polarizable Continuum Model Time Dependent Density Functional Theory Approach. *J. Chem. Phys.* **2007**, *127*, 074504.
(60) Frisch, M. J.; Trucks, G. W.; Schlegel, H. B.; Scuseria, G. E.; Robb, M. A.; Cheeseman, J. R.; Scalmani, G.; Barone, V.; Mennucci, B.; Petersson, G. A et al. *Gaussian 09*, Revision A.2; Gaussian, Inc.: Wallingford, CT, 2009.
(61) Aquilante, F.; De Vico, L.; Ferré, N.; Ghigo, G.; Malmqvist, P. A.; Neogrady, P.; Pedersen, T. B.; Pitonak, M.; Reiher, M.; Roos, B. O.; et al. Software News and Update MOLCAS 7: The Next Generation. *J. Comput. Chem.* **2010**, *31*, 224−24.
(62) Ghigo, G.; Roos, B. O.; Malmqvist, P.-Å A Modified Definition of the Zeroth-Order Hamiltonian in Multiconfigurational Perturbation Theory (CASPT2). *Chem. Phys. Lett.* **2004**, *396*, 142−149.
(63) Asplund, M. C.; Zanni, M. T.; Hochstrasser, R. M. Two-Dimensional Infrared Spectroscopy of Peptides by Phase-Controlled Femtosecond Vibrational Photon Echoes. *Proc. Natl. Acad. Sci. U.S.A.* **2000**, *97*, 8219−8224.
(64) Becker, R. S.; Freedman, K. A Comprehensive Investigation of the Mechanism and Photophysics of Isomerization of a Protonated and Unprotonated Schiff Base of 11-*cis*-Retinal. *J. Am. Chem. Soc.* **1985**, *107*, 1477−1485.
(65) Freedman, K. A.; Becker, R. S. Comparative Investigation of the Photoisomerization of the Protonated and Unprotonated n-butylamine Schiff Bases of 9-*cis*-, 11-*cis*-, 13-*cis*-, and All-*trans*-Retinals. *J. Am. Chem. Soc.* **1986**, *108*, 1245−1251.
(66) Hu, Y.; Okumura, A.; Koyama, Y.; Yamano, Y.; Ito, M. Effects of the Terminal-Methyl Position and of the Length of the Conjugated Chain on the *cis*-Isomers Produced by Photo-Isomerization: Analysis by HPLC and Configurational Determination by ^{1}H NMR Spectroscopy of Isomeric Analogues of Retinal and *β*-Apo-12′-carotenal. *Spectrochim. Acta, Part A* **1997**, *53*, 913−926.
(67) Starcke, J. H.; Wormit, M.; Schirmer, J.; Dreuw, A. How Much Double Excitation Character do the Lowest Excited States of Linear Polyenes Have? *Chem. Phys.* **2006**, *329*, 39−49.
(68) Angeli, C.; Improta, R.; Santoro, F. On the Controversial Nature of the $^1B_{1u}$ and $^2B_{1u}$ States of *trans*-Stilbene: The *n*-Electron Valence State Perturbation Theory Approach. *J. Chem. Phys.* **2009**, *130*, 174307.
(69) Angeli, C.; Pastore, M. The Lowest Singlet States of Octatetraene Revisited. *J. Chem. Phys.* **2011**, *134*, 184302.
(70) Snyder, R.; Arvidson, E.; Foote, C.; Harrigan, L.; Christensen, R. L. Electronic Energy Levels in Long Polyenes: S2 → S0 Emission in All-*trans*-1,3,5,7,9,11,13-Tetradecaheptaene. *J. Am. Chem. Soc.* **1985**, *107*, 4117−4122.
(71) Knecht, S.; Marian, C. M.; Kongsted, J.; Mennucci, B. On the Photophysics of Carotenoids: A Multireference DFT Study of Peridinin. *J. Phys. Chem. B* **2013**, *117*, 13808−13815.
(72) Angeli, C. On the Nature of the $\pi \rightarrow \pi^*$ Ionic Excited States: The V State of Ethene as a Prototype. *J. Comput. Chem.* **2009**, *30*, 1319−1333.
(73) Yamaguchi, S.; Tahara, T. Two-Photon Absorption Spectrum of All-*trans*-Retinal. *Chem. Phys. Lett.* **2003**, *376*, 237−243.
(74) Polivka, T.; Zigmantas, D.; Frank, H. A.; Bautista, J. A.; Herek, J. L.; Koyama, Y.; Fujii, R.; Sundström, V. Near-Infrared Time-Resolved

Study of the S1 State Dynamics of the Carotenoid Spheroidene. *J. Phys. Chem. B* **2001**, *105*, 1072−1080.
(75) Vivas, M. G.; Silva, D. L.; Boni, L.; Zalesny, R.; Bartkowiak, W.; Mendonca, C. R. Two-Photon Absorption Spectra of Carotenoids Compounds. *J. Appl. Phys.* **2011**, *109*, 103529.
(76) Marian, C. M.; Gilka, N. Performance of the Density Functional Theory/Multireference Configuration Interaction Method on Electronic Excitation of Extended Systems. *J. Chem. Theor. Comp.* **2008**, *4*, 1501−1515.
(77) Schmidt, M.; Tavan, P. Electronic Excitations in Long Polyenes Revisited. *J. Chem. Phys.* **2012**, *136*, 124309.
(78) Orlandi, G.; Zerbetto, F. Vibronic Coupling in Polyenes: The Frequency Increase of the Active C═C ag Stretching Mode in the Absorption Spectra. *Chem. Phys.* **1986**, *108*, 187−195.
(79) Zerbetto, F.; Zgierski, M. Z.; Orlandi, G.; Marconi, G. Vibronic Coupling in Polyenes and their Derivatives. Interpretation of the Absorption and Emission Spectra of a Derivative of Dodecahexaene. *J. Chem. Phys.* **1987**, *87*, 2505−2512.
(80) Mimuro, M.; Nishimura, Y.; Yamazaki, I.; Katoh, T.; Nagashima, U. Fluorescence Properties of the Allenic Carotenoid Fucoxanthin: Analysis of the Effect of keto Carbonyl Group by Using a Model Compound, All-*trans*-*β*-apo-8′-carotenal. *J. Lumin.* **1992**, *51*, 1−10.
(81) Niedzwiedzki, D. M.; Kajikawa, T.; Aoki, K.; Katsumura, S.; Frank, H. A. Excited States Energies and Dynamics of Peridinin Analogues and the Nature of the Intramolecular Charge Transfer State in Carbonyl-Containing Carotenoids. *J. Phys. Chem. B* **2013**, *117*, 6874−6887.
(82) Merchan, M.; Gonzalez-Luque, R. Ab Initio Study on the Low-Lying Excited States of Retinal. *J. Chem. Phys.* **1997**, *106*, 1112−1122.
(83) Nagae, H.; Kuki, M.; Zhang, J.-P.; Sashima, T.; Mukai, Y.; Koyama, Y. Vibronic Coupling through the In-Phase, CC Stretching Mode Plays a Major Role in the $2Ag^-$ to $1Ag^-$ Internal Conversion of All-*trans*-Carotene. *J. Phys. Chem. A* **2000**, *104*, 4155−4166.
(84) Wagner, N. L.; Greco, J. A.; Enriquez, M. M.; Frank, H. A.; Birge, R. R. The Nature of the Intramolecular Charge Transfer State in Peridinin. *Biophys. J.* **2013**, *104*, 1314−1325.